U.PORTO
FEUP FACULDADE DE ENGENHARIA
UNIVERSIDADE DO PORTO

Department of Mechanical Engineering

Integrated Masters in Mechanical Engineering

Strength of Hybrid Laminates Aluminium Carbon-Fibre Joints with Different Lay-up Configurations

Submitted by:

Miguel Pereira Palmares

Supervised by:

Lucas Filipe Martins da Silva

Co-supervised by:

Ricardo João Camilo Carbas

July 2016

Abstract

The use of composite materials in industry is growing due to various technological advances in composite materials, accompanied by improvements in the structural adhesives used to bond them. Fibre metal laminates (FML's) are hybrid composite structures based on thin sheets of metal alloys and plies of fibre reinforced polymeric materials. The fibre/metal composite technology combines the advantages of metallic materials (high bearing strength, impact resistance and reparability characteristics) and fibre reinforced matrix systems (high strength and stiffness, fatigue and corrosion characteristics). Due to their advantages, FML's are finding great use in many aerospace applications.

The aim of the present project was to use a concept similar to that used in FML to increase the peel strength of composite materials and increase the joint strength of composite adhesive joints. Carbon fibre reinforced polymer (CFRP) composites were modified by including one and two aluminium sheets during the laminate manufacture to enhance the composite through-thickness properties. The objective was to identify the joint configuration that gives the best joint strength improvement in relation to the CFRP-only reference joint. An adhesive developed for the aeronautical industry, 3M AF 163-2K, was chosen to manufacture single lap joints (SLJ's) for tensile testing.

The joint strength of four different lay-up configurations was evaluated by performing tensile tests of SLJ's. Tensile and shear properties of the adhesive, as well as the fracture energies in mode I and II were determined via Bulk, TAST, DCB and ENF test, respectively. Finite element analysis (FEA) using Abaqus was carried out to predict the failure load and the failure type of each solution.

The delamination of the SLJ was less severe using the aluminium-carbon fibre laminates, while an increase of the joint strength was verified specimens for longer overlaps. The numerical models correlated well with the experimental data.

Resumo

O uso de materiais compósitos tem vindo a aumentar devido aos avanços tecnológicos verificados não só neste tipo de materiais mas também nos adesivos estruturais. Os *Fibre-Metal Laminates* (FML) são compósitos híbridos que consistem numa estrutura composta por lâminas finas de uma liga metálica com camadas de um polímero reforçado com fibras. Esta tecnologia permite combinar as características dos metais (resistência ao impacto e aos entalhes, facilidade de reparação) com as vantagens dos polímeros reforçados com fibras (elevada resistência mecância e rigidez, boa resistência à fadiga e à corrosão). Os FML têm vindo a ser cada vez mais utilizados para aplicações aeronaúticas e aeroespaciais.

O objectivo deste projeto é utilizar um conceito similar ao dos FML para melhorar a resistência ao arrancamento de materiais compósitos e à resistência das juntas adesivas com este tipo de materiais. Os compósitos produzidos de plástico reforçado com fibra de carbono (CFRP) foram modificados com a inclusão de uma e duas lâminas de alumínio de forma a melhorar as propriedades transversais do laminado. O objectivo é identificar a configuração que permite obter as melhores propriedades relativamente a uma configuração que utiliza apenas CFRP. Para a produção das juntas de sobreposição simples (SLJ), um adesivo muito utilizado na indústria aeronáutica foi escolhido, o 3M AF 163-2K.

A resistência de quatro configurações diferentes foi estudada através a ensaios de tracção de SLJ's. As propriedades à tracção e ao corte do adesivo, bem como as energias de fratura em modo I e II foram determinadas recorrendo a ensaios Bulk, TAST (*Thick Adherend Shear Test*), DCB (*Double Cantilever Beam*) e ENF (*End-notched flexure*), respectivamente. Para obter uma previsão da força de rutura e do tipo de rutura de cada configuração recorreu-se a uma análise de elementos finitos utilizando o software comercial Abaqus®.

A delaminação das SLJ's foi menos grave quando laminados de alumínio-fibra de carbono foram utilizados, verificando-se ainda um aumento da resistência da junta para todas as configurações. Os modelos numéricos tiveram uma boa concordância com os resultados experimentais obtidos, quer a nível da previsão da força quer no tipo de rutura.

Acknowledgments

I would like to thank firstly to Ricardo Carbas, for his guidance, patience and dedication during this months, and the time and effort invested in this project.

I would like also to thank Professor Lucas da Silva, for sharing his vast knowledge and expertise during this dissertation.

To all the members of ADFEUP, particularly my fellow Master's colleagues, for the many hours spent together and for all their help and advice during this semester.

I would like to thank my friends, Bruno, Francisco, Inês, Paulo e Tiago, for their friendship and support, for making this journey easier since the beginning, and for the countless moments and memories that we shared.

Finally, to my family, especially my mother, who supported me no matter what, for being there whenever I needed, and without whom I would have never become an engineer.

Contents

List of Figures

List of Tables

Nomenclature

Acronyms

CBBM	Compliance-Based Beam Method
CFRP	Carbon Fibre Reinforced Plastic
CTE	Coefficient of Thermal Expansion
CZE	Cohesive Zone Elements
DCB	Double Cantilever Beam
ENF	End Notched Flexure
FEA	Finite Element Analysis
FPZ	Fracture Process Zone
R-Curve	Resistance Curve
SLJ	Single Lap Joint
TAST	Thick Adherend Shear Test

Symbols

E	Young's Modulus
G	Shear Modulus
ν	Poisson's Ratio
P	Load

δ	Displacement
b	Width of the joint
t	Thickness of the adherend
l	Overlap length
a_{eq}	Equivalent crack length
E_f	Corrected flexural modulus
G_{IC}	Fracture energy in mode I
G_{IIC}	Fracture energy in mode II

1. Introduction

1.1. Background and motivation

The use of composite materials have increased exponentially throughout the years. The combination of excellent mechanical properties with a low weight makes this materials a natural alternative to metallic alloys in the transport industry. Nowadays these materials have a competitive price and compete with metallic alloys in a wide range of applications, from the aerospace industry to the automotive industry or even sports goods.

The adhesion bonding technology has grown in pair with composite materials. Composite materials have shown a massive decrease in their mechanical properties when holes are cut with the purpose of joining using rivets or bolts due to the low bearing and shear strengths and the higher notch sensitivity when compared to metals [1]. Hence, the advances in adhesive bonded joints made possible the use of this materials in large scale.

Because most of the fibre reinforced plastics, the most common type of composite materials used the industry, do not show an isotropic behaviour, research has been done in order to increase the mechanical properties in different directions. Besides the usual loadings in out of plane directions in composites, bonded joints experience peel loading, so the composite may fail in transverse tension before the adhesive fails. In order to increase the peel strength of the composite and to avoid delamination, several techniques have been proposed, such as internal taper and adhesive fillet or z-pins mounted transversally to the direction of the fibres in the composite [2, 3].

Another solution is to use a concept similar to FML, vastly used in the aeronautical industry to increase the fatigue resistance of the metal. FML are hybrid composite structures where plies of fibre reinforced plastic and sheets of a metallic alloy

are stacked alternately. This allow to combine the properties of the metallic material, such as the high bearing strength, impact resistance and an easier reparability, with the properties of the plastic reinforced composites like the excellent fatigue and corrosion resistance and the high strength and stiffness [4]. In this project, the objective is to use a concept similar to that used in FML to improve the peel strength of the composite materials, and increase the joint strength of composite adhesive joints.

1.2. Objectives

The main objective of this thesis is to find an optimal FML configuration that shows the best improvement in the peel strength of the composite over the CFRP-only composite. To determine the best configuration, different combinations hybrid aluminium-carbon fibre laminates are studied and tested by performing tensile tests of SLJ's using this materials.

1.3. Research methodology

In order to achieve the aim of the thesis, the following work plan was executed:

1. A literature review on adhesive bonding, composites and FML and the failure mechanisms of SLJ's.
2. Characterization of the selected adhesive with the purpose of determine the cohesive laws required for the numerical simulation.
3. Manufacture of FML specimens and SLJ's.
4. Numerical simulation of the tensile testing of SLJ's using FEA to correlate and validate the experimental results.

5. Perform the tensile tests of SLJ's for different combinations of aluminium-carbon fibre laminates, and analyse the fracture surfaces and the load vs displacement curves.

1.4. Outline of the thesis

This thesis comprehends seven major chapters. In the first one, an introduction to the thesis and its purpose are presented, as well as the main objectives and the workflow that was followed.

The second chapter consists on a literature review on adhesive bonding and composites, namely CFRP and FML, with attention to the failure mechanisms of both adhesives and composites.

In the third chapter, the technical details and the experimental procedures are described.

The fourth chapter regards the experimental results for the characterization of the adhesive.

In the fifth chapter the results for the tensile testing of SLJ's are presented and discussed, including the fracture surfaces and the load-vs displacement curves.

The sixth chapter regards the finite element analysis, with an explanation of the models developed for this project.

In the seventh chapter, the results from both FEA and from the tensile tests are compared and discussed.

The eighth chapter presents the conclusions drawn from the work developed in this study.

The ninth chapter suggests future investigations and ideas to follow the work of this thesis.

2. Literature review

2.1. Adhesive bonding

Adhesive bonding is a material joining process that consists in the bonding of two different materials through the solidification of an adhesive between them, where mechanical force or work can be transferred across the interface [5]. An adhesive is then a material that when is applied to surfaces of materials can join them together and resist separation [6]. This technology, when in comparison to riveting or fastening, the most common material joining processes, has many advantages that have been explored by different industries, mainly the automotive and the aeronautical ones.

Adhesive bonded joints have been successfully used for hundreds of years in different applications, from domestic utensils and sports goods to the transports industry. Bonding has been used since the Mesopotamians and Sumerians in 3000 BC, using asphalt for construction purposes and glue from animal skins, respectively [7]. Only in the beginning of the twentieth century polymeric-based adhesives began to be commercially available, due to technological developments verified throughout this time. Up until this time, only glues made from natural materials were being used. The first synthetically produced polymer to be patented as an adhesive was a phenolic resin in 1909, by Baekeland [7]. After this milestone was achieved, other materials were discovered and different types of curing processes were improved. Table 1 gives an overview on the developments made in the twentieth century [7, 8].

This developments allowed for a better understanding of this type of materials and therefore an increased security when using them. Nowadays, adhesives are preferred over other bonding technologies in various applications, not only for domestic utensils that do not require good mechanical properties, but also for more demanding applications.

Table 1 - Developments in the adhesive industry during the twentieth century

Decade	**Adhesive**
1920s	Cellulose ester, alkyd resin, cyclized rubber in adhesives, polychloroprene (neoprene), soybean adhesives
1930s	Urea-formaldehyde, pressure-sensitive tapes, phenolic resin adhesive films, polyvinyl acetate wood glues
1940s	Nitrile-phenolic, vinyl-phenolic, acrylic polyurethanes
1950s	Epoxies, cyanoacrylates, anaerobic, epoxy alloys
1960s	Polyimide, polybenzimidazole
1970s	Second-generation and pressure-sensitive acrylics, structural polyurethanes
1980s	Toughеners for thermoset resins, water-borne epoxies, water-borne contact adhesives, formable and foamed hot melts
1990s	Polyurethane-modified epoxy, curable hot melts, UV and light cure systems
2000s	Water borne adhesives, reduced volatile organic compounds, solvent-free one- and two-part adhesives

The adhesives can be divided accordingly to their chemical composition, but can also be distinguished between non-structural and structural. An adhesive to be considered structural needs to be able to transfer loads between the substrates without losing its integrity within the design limits, and be able to withstand a shear load higher than 7 MPa [9]. This type of adhesive is of most interest to the industry, and the development of bonds using this materials is a constant challenge for scientists and engineers. The

most common type of structural adhesives are presented in Table 2, as well as their major properties [4, 7, 10].

Table 2 - Most important groups of adhesives and their properties

Adhesive	**Advantages**	**Disadvantages**
Epoxies	High strength, good toughness, temperature resistance and relatively low cost	Short pot life, exothermic reaction, requires precise chemical formulation
Polyurethanes	Good strength and toughness at low temperatures, resistance to fatigue, impact resistance, good durability	Moisture sensitive, poor heat resistance, short pot life
Phenolics	High hardness, excellent thermal stability, cheap	Brittle with low peel strength, requires very high cure pressures
Silicones	Environmental stability, high degree of flexibility, capability to bond materials of various natures, excellent resistant to heat and moisture	High cost, lower mechanical properties at room temperature
Cyanoacrylates	Rapid room-temperature cure, good mechanical strength, long pot life, good adhesion to metal	Expensive, poor durability, poor heat resistance
Modified acrylics	Good peel and shear strengths, does not require an extensive surface treatment, room temperature cure	Limited resistance to thermal chock, difficult to process, toxic and flammable
Aromatics	Very good heat resistance, aerospace applications	Expensive, hard to process, very brittle at room temperature

2.1.1. Advantages

Despite the fact that adhesives have a lower mechanical strength in comparison to metals, because it is possible to have a bigger bearing area between the materials, a higher stiffness and a more uniform stress distribution can be achieved, reducing also the stress concentration caused by the bolts and rivets (Figure 1) [11]. The superior stress distribution also improves the fatigue strength of the joints, since the stress concentration caused by the rivet and bolt holes is not existent.

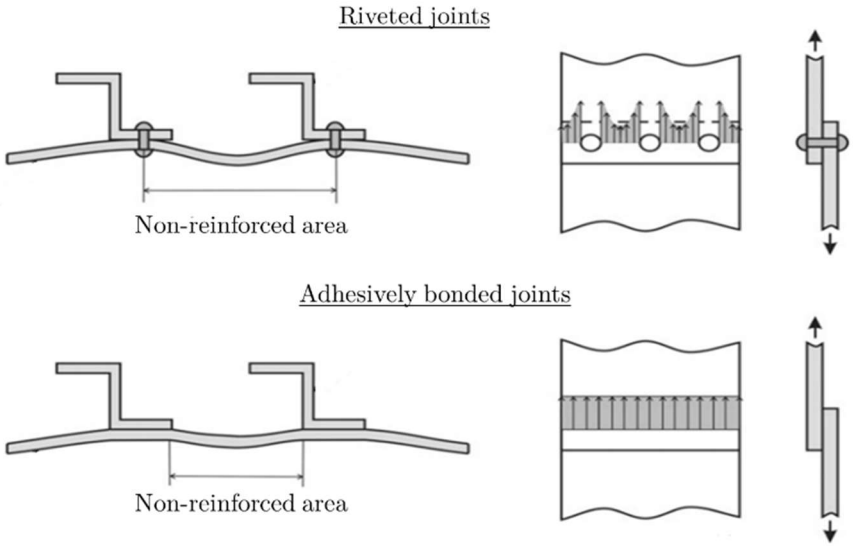

Figure 1 - Improved stiffness (left) and stress distribution (right) of adhesively bonded joints in relation to riveted joints [11]

Adhesives also give the possibility of bonding different types of materials, or materials with a big difference in properties such as the thermal expansion coefficient. Also, due to the low stiffness or the brittleness of certain materials, i.e. thin metallic sheets or ceramic materials, respectively, bolting and riveting cannot be applied to certain structures. For instance, using bolts or rivets it would not be possible to bond a metal and a ceramic. However, it is possible to bond these materials using adhesives, inclusively for applications at very high temperatures [12].

Another major advantage of adhesives is their low weight, due to their polymeric nature. The automotive and aerospace industries, for example, continue to develop

technologies with the sole purpose of reducing the weight of vehicles, and therefore reducing fuel consumptions and the emission of combustion products. The use of this type of materials contributes to a weight reduction when in comparison with metallic bolts and rivets.

Vibration damping is another important advantage of adhesive joints. Relatively to the traditional bonding technologies, adhesively bonded joints can deform and regain the initial configuration unlike other joining methods, as they can deform elastically much more easily [13].

Regarding adhesives and other polymers in general, the damping characteristics have also a relevant role for other purposes. As it is known, the glass transition temperature is one of the most important properties of a cured adhesive [14]. It defines the transition between a rubbery and a vitreous state of an amorphous solid. It is important to understand the behaviour of the adhesives below and above this temperature, since its mechanical properties change drastically with this transition [15].

In order to determine this temperature, an intrinsic property of polymers in general, several techniques have been developed throughout the years, such as the DSC (differential scanning calorimetry), TMA (thermos-mechanical analysis) and DMA (dynamic mechanical analysis). Adams et al. [16] developed a technique of determining the glass transition temperature of adhesives in an easier and faster way than the conventional methods, taking advantage of the damping properties of the adhesives to better characterize their behaviour. This techniques has already been used to develop a fully functional apparatus, better described in [15].

2.1.2. Disadvantages

Despite these advantages, the susceptibility of adhesives to both temperature and humidity due to its polymeric nature is something that cannot be overcome easily [17]. Also, in order to achieve good adhesion, the surfaces that will be bonded need to be properly prepared using mechanical abrasion, degreasing with a solvent, chemical etching

or anodizing, among others. The need of this preparation, combined with the need of fixing the materials during the cure of the adhesive could have a big impact in the efficiency of the production line.

The quality control of this kind of bonds is still difficult to perform with non-destructive techniques. These disadvantages encourage engineers to continue to study this type of bonding and develop new techniques to increase both its efficiency and economic feasibility.

Besides the service conditions at which the adhesive joint will be, the type of load has also a major influence. Adhesive joints are normally stressed in 4 different ways (Figure 2):

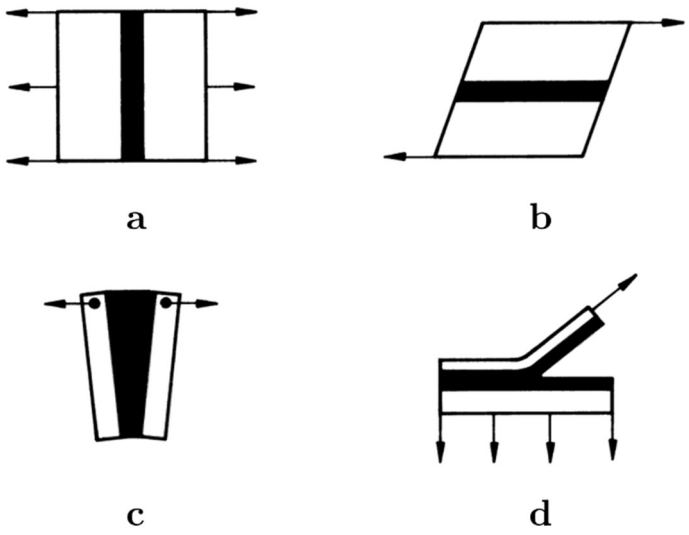

Figure 2 - Typical loads of bonded joints: (a) normal stress, (b) shear stress, (c) cleavage, (d) peel stress [6]

-Normal or direct stresses (tensile or compressive load). These stresses are uniformly distributed across the bonded area, and are normal to the plane on which they act.

-Shear stresses. In this case the adherends are translated across the adhesive while remaining parallel (these stresses are parallel to the plane on which they act). A well designed adhesive joint loads the adhesive with shear stresses.

-Peel stresses. This kind of stresses appear when one or both of the adherends are ductile, and concentrates the stresses along a thin line. A joint is designed to specially avoid this kind of stresses, which are even more relevant when the adherends are composites.

-Cleavage stresses. One of the adherends is subjected to stress while the other is theoretically under no stress, typically from a tensile force or bending moment, or when both materials are stiff.

It is quite challenging to design a joint with only one type of stress present. The main goal is to avoid peel stresses, but usually the stress state of the joint is a combination of different types of loads. Because it is impossible to avoid certain types of forces, different measures need to be taken to increase the strength of the joint.

2.1.3. Joint configuration

Successfully joining structural panel components can be achieved through different ways, whether it is in the automotive or in the aeronautic industry, or even in civil engineering applications. Each joint configuration has its advantages and disadvantages. The major differences between each one of them are in the ease of manufacture and in the introduction of stress concentrations. There are two major groups: the ones initially designed to bond structural components (Figure 3 – a, b, c, d), and the ones used to repair defects such as crack and ballistic damage (Figure 3 – e, f, g, h) [11].

The most used in the industry and in the test standards are the SLJ, due to their simplicity and effectiveness. Other configurations are also worth mention such as the butt joints, the tubular laps, the corner joints and the tabular lap.

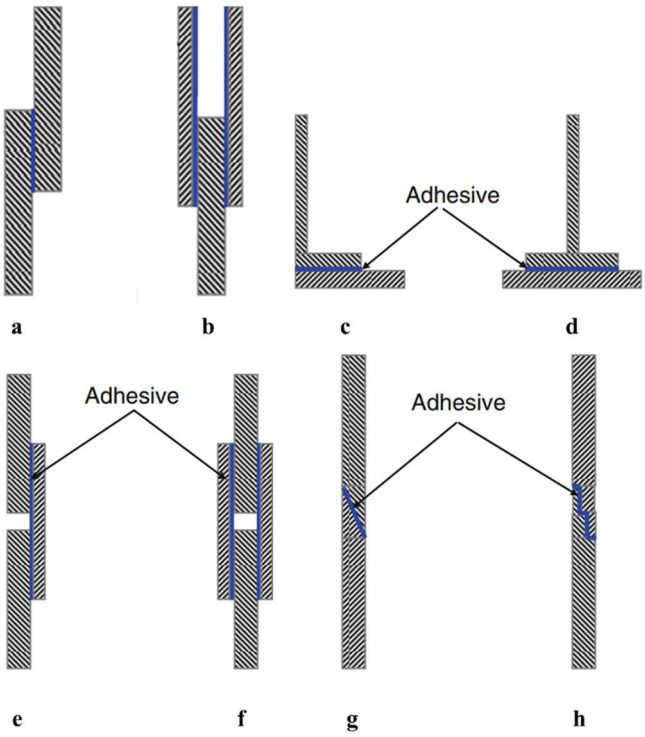

Figure 3 - Adhesive bonded joints configuration: (a) single lap joint; (b) double lap joint; (c) L-joint; (d) T-joint; (e) single strap joint; (f) double strap joint; (g) scarf joint; (h) step joint [11]

2.2. Failure modes

The failure of adhesives joints can occur due to different reasons that depend on the services conditions and the preparation of the bond. The service temperature and humidity, the magnitude of the load and how it is applied to the joint have to be taken into consideration, as well as the surface treatments applied to the adherends. Surface treatments are considered mostly for durability purposes rather than increasing the bond strength, and have a big impact on the behaviour of the joint at long term. In order to understand the types of bond failure, it is necessary to define two concepts, adhesion and cohesion.

Adhesion refers to the state in which two dissimilar bodies are held together by intimate interfacial forces such as Van der Waals forces, chemical bonding or electrostatic attraction, and allow mechanical forces to be transferred across the interface [5]. On the

other side, cohesion is the state in which the particles on single substance are held by intermolecular forces [9]. Having taken this concepts into consideration, it is possible to identify three major types of bond failure (Figure 4):

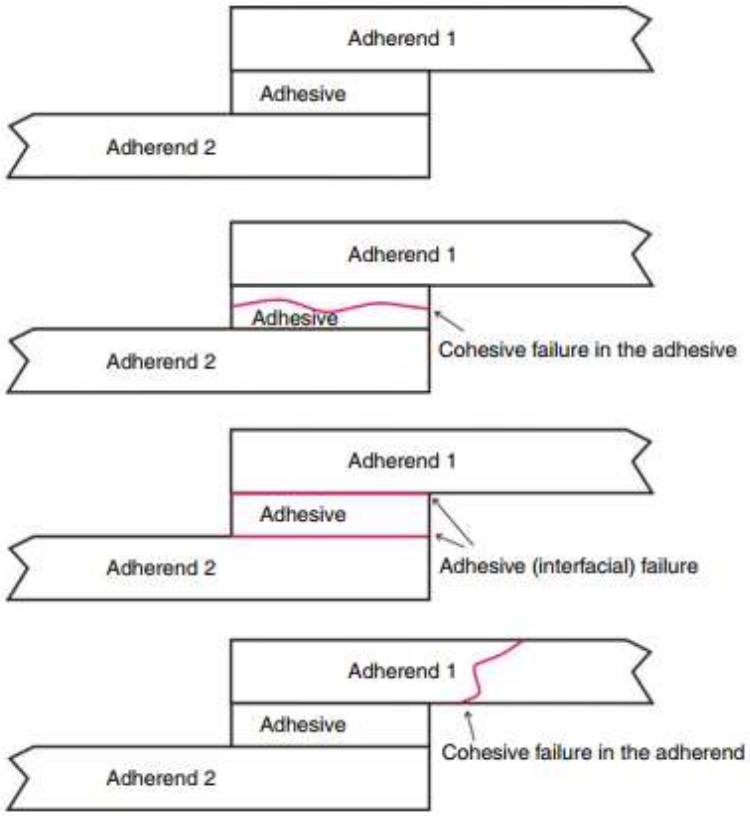

Figure 4 - Examples of cohesive and adhesive failures [11]

-Cohesive failure in the adherend: the failure occurs in the adherend, outside of the bonded area, indicating that the adhesive used and the bond interface are more resistant than the adherend. When this type of failure is identified, an adherend with superior mechanical properties is needed in order to take maximum advantage from the adhesive and avoiding damage the adherends, usually more expensive and more difficult to manufacture.

-Cohesive failure in the adhesive: fracture of the adhesive layer. The strength of the adhesive is lower than the adherend and the interface between them. The joint is properly designed with the adhesive withstanding all the load. The main goal when designing an adhesively bonded joint is to promote a cohesive failure.

-Adhesive failure: the failure occurs in the interface between the adhesive and the adherend, usually indicates a poor adhesion between the materials that might be due to an inappropriate surface preparation

In many practical cases there is not a clear failure mode, but a mixture of more than one. A mixed failure is then evaluated through the percentage of cohesive or adhesive failure, determined by the bonded area that has failed either cohesively or adhesively [9].

2.3. FRP

The use of composite materials, especially the fibre reinforced plastics (FRP), have increased exponentially since the twentieth century. The superior mechanical properties such as stiffness and ultimate strength or fatigue resistance combined with an extremely low weight are characteristics very interesting for the transportation industry (Figure 5).

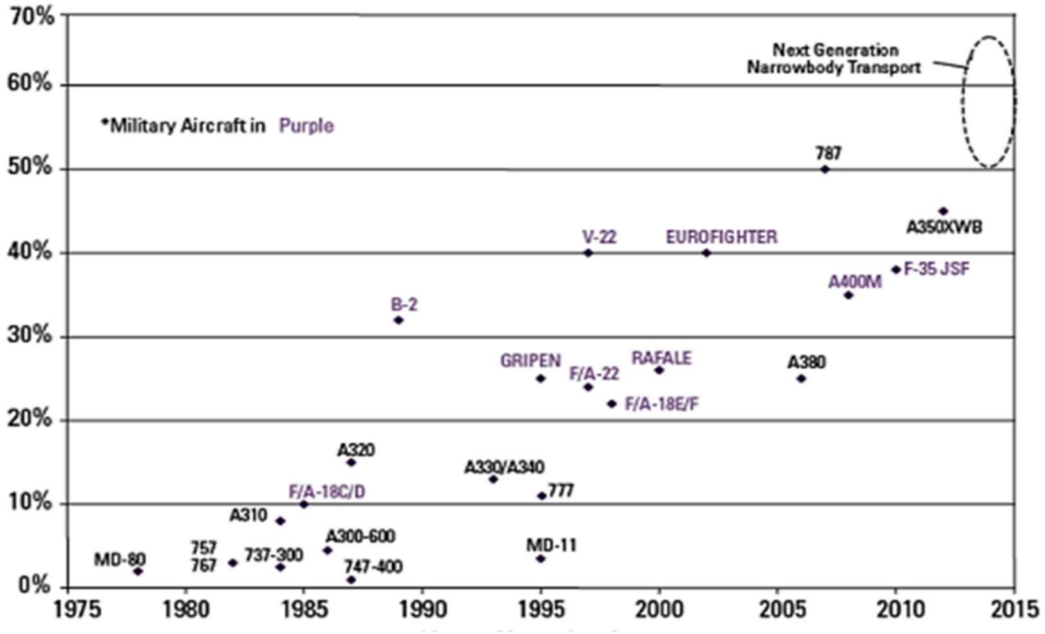

Figure 5 - Percentage of composite components in aircrafts throughout the years [18]

This type of composites are usually composed of unidirectional or woven fibres, usually made from glass, carbon or aramid, that reinforce a polymer, normally a thermosetting matrix such as an epoxy resin. Nowadays the use of thermoplastic resins such as polyetherethreketone (PEEK) and polyamides is increasing but the price and the lack of data regarding this materials are still drawbacks difficult to overcome [19]. The fibres are responsible for properties such as stiffness, tensile strength and fatigue resistance, while the resin makes the composite tough and bonds the fibres. The properties of the composite depend obviously on the mechanical properties of both the fibres and the resin, but also on the volume ratio between them and the length and orientation of the fibres [20]. These materials present an anisotropic behaviour: because of the orientation of the fibres, the properties along the fibre direction are vastly superior to the properties in the transverse direction, where the stiffness and the shear strength are much lower. This difference, when in comparison to isotropic materials like metals, cannot be neglected and needs to be taken into consideration [21].

2.3.1. Failure in composite adherends

Because of its nature, composites may fail through three different mechanisms (Figure 6):

-tensile failure in the fibre direction (fibre rupture). This is due to longitudinal compression in the fibre direction, causing a brittle failure of the fibre.

-tensile failure perpendicular to the fibre direction (matrix failure). The forces applied to the composite exceed the limits of the matrix, separating the fibres from the matrix.

-interlaminar shear failure (delamination). Usually caused by loads applied in the through-thickness direction of the laminate causing the material to shear at the interface between matrix and fibres. For unidirectional composites, the most common failure type is delamination, when two adjacent plies of the composite are separated.

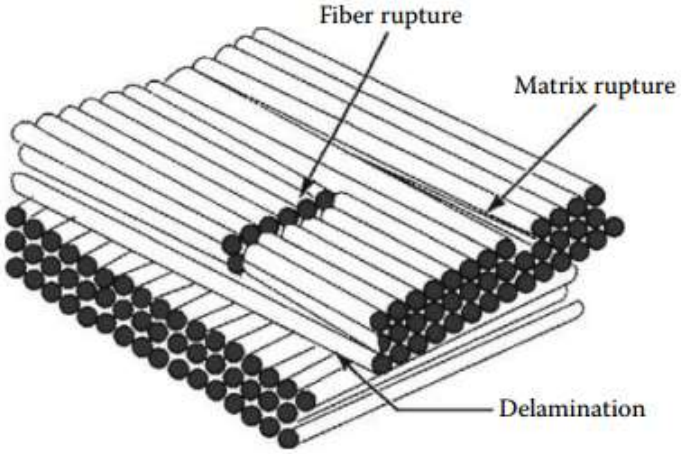

Figure 6 - Different types of failure [20]

Regarding adhesively bonded joints with FRP adherends, there are several failure modes, namely: adhesive failure, cohesive failure, thin-layer cohesive failure, fibre-tear failure, light-fibre-tear failure, stock-break failure or mixed failure (Figure 7) [22].

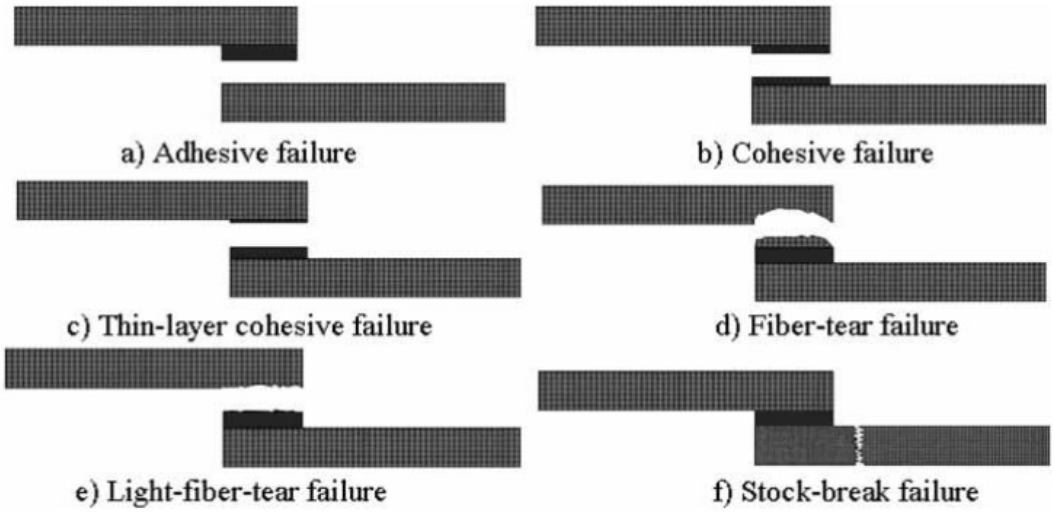

Figure 7 - Failure modes for FRP adhesively bonded joints [22]

When adhesively joined, the composite adherends experience peel loading, with its peak at the edges of the bonded area. Because of the low transverse tensile strength

in the through-thickness direction, the failure of the composites is most likely to occur at the ends of the overlap length (Figure 8) [3].

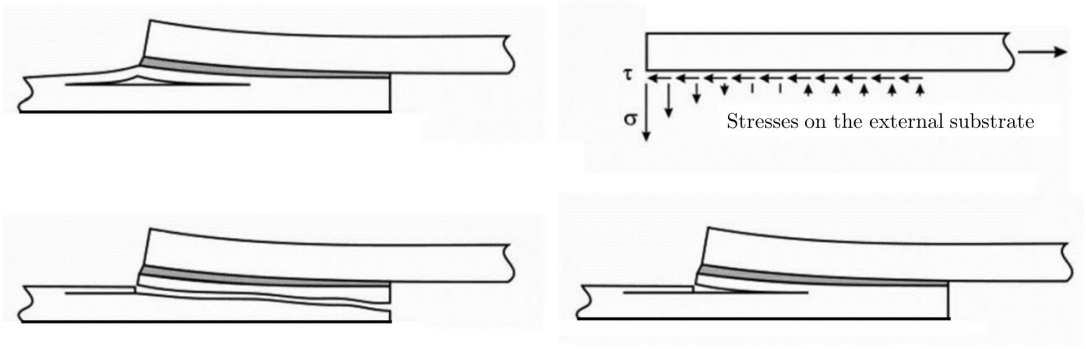

Figure 8 - Peel stress failure of composite adherends [23]

With the purpose of increasing the peel strength of composites, several techniques have been proposed. da Silva et al. [3] proposed an internal taper and an adhesive fillet. This techniques showed an increase in the failure load of the joint, however its manufacture is quite difficult and time consuming. Other technique to increase the through-thickness strength of the composite is z-pins (Figure 9). This technique was developed in the 1970s, and consists on inserting thin rods made from a high strength material with 0.2 to 1 mm thickness, and with a volume content ranging from 0.5 to 4%. The results using this technique have been promising, with benefits such as improved delamination resistance, damage tolerance and through-thickness stiffness. Further investigation regarding the durability of this solution under real conditions is still needed [2].

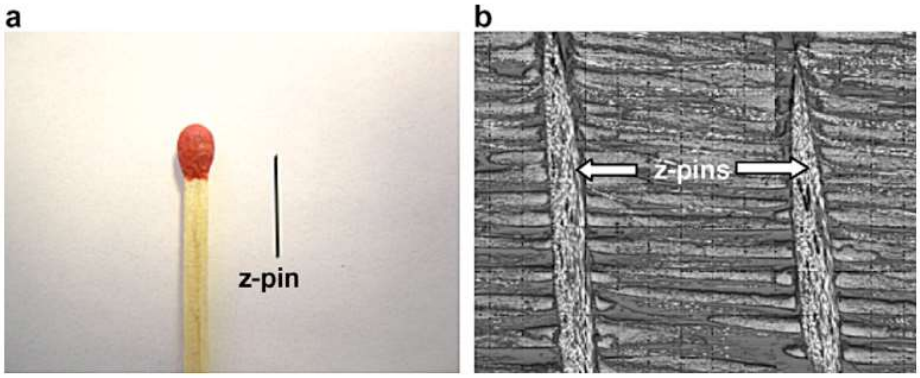

Figure 9 - (a) Relative size of a z-pin; (b) z-pins located inside a FRP composite [2]

The main objective of this thesis is to increase the peel strength of the composite by using a concept similar to the FML.

2.3.2. FML

FML were invented by Professor Bond Vogelesang of the Aerospace Faculty of the Technical University of Delft, in the 1980s, where it was found that the fatigue crack growth rates in adhesive bonded sheet materials could be reduced by laminating and adhesively bonding thin sheets of the material [4]. After some further development and optimization of the concept the differences in the fatigue life between an aluminium alloy sheet and a composite laminate were very significant (Figure 10).

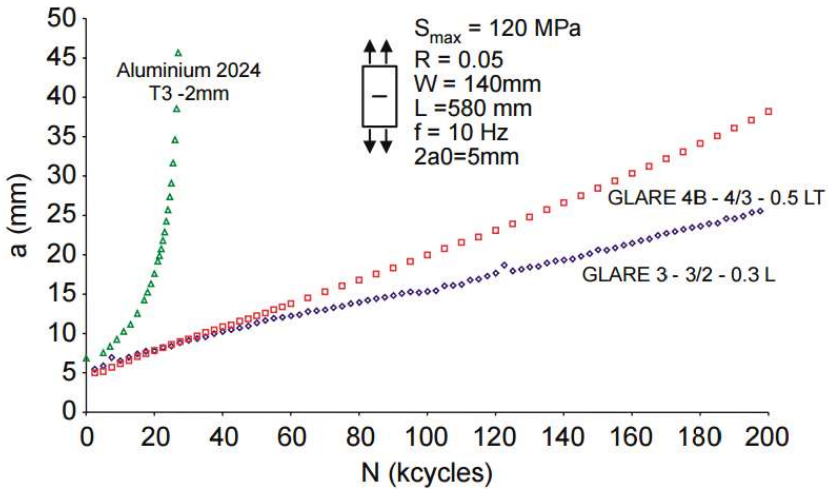

Figure 10 - Crack growth curves of aluminium 2024-T3, Glare 3-3/2-0.3 L and Glare 4B-4/3-0.5 LT for constant amplitude fatigue loading [24]

FML belong to the class of hybrid composites, and consist on a fibre reinforced plastic interleaved with thin sheets of a metallic alloy. The first types of FML developed were ARALL (Aramid Reinforced Aluminium Laminate) and later GLARE (Glass reinforced aluminium). The idea of the concept was to put together the best of both composites and metals, and obtain a material superior to a fibre-reinforced plastic or an aluminium alloy. Because of the different types of metallic alloys and FRP, as well as the different stacking orders possible, there is a virtually infinite number of combinations

possible for FMLs [25]. Nowadays, FML is an established solution for the aerospace and aeronautical industries, being used in the fuselage of the most recent planes like the A380 or the Boeing 787 Dreamliner (Figure 11).

One type of FML that is not as developed as GLARE or ARALL is the CARALL (carbon fibre aluminium laminates). This type of laminates are expected to have superior properties to the other types of FML because of the carbon fibre, such as the high stiffness and specific strength. However, this type of laminates don't work as well as the other because of the difference in the thermal expansion coefficients of CFRP and aluminium. This leads to high thermal stresses during the cure of the composite, reducing the fatigue strength of the FML [27]. Also, the fact that an epoxy based composite is used leads to a longer curing process, which can affect the economic feasibility of FML. In order to further improve FML, there are new studies and new technologies being developed. The use of titanium instead of aluminium, which has a lower thermal expansion coefficient, results in lower residual stresses and an increased mechanical strength. Also, some reinforced plastics using thermoplastic resins are also being tested, not only reducing the processing time but also offering better reparability and superior interlaminar fracture properties [1, 28, 29].

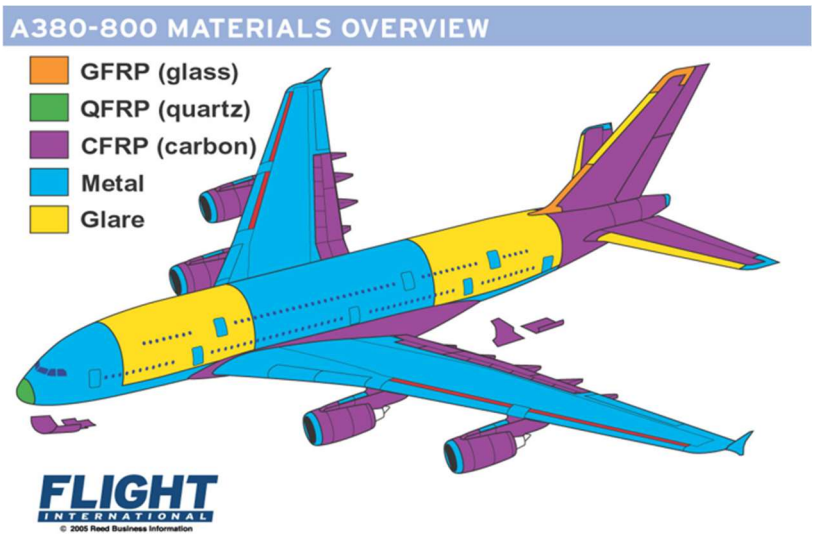

Figure 11 - Different types of materials used in the A380-800 [26]

2.4. Surface treatments

Surface treatments are an essential step in the manufacture of adhesively bonded joints, since the bond strength and the durability of the joint are critically dependent on the interaction between the adhesive and a pre-treated adherend [30]. Usually the preparation of surfaces involves removing the existent contaminated layers which do not promote bonding between the adhesive and the adherend, the so called weak boundary layers, and allow the adhesive and the adherend surface to contact directly [9]. By increasing surface tension, increasing surface roughness, and changing surface chemistry, a more intimate bond can be formed, which allows for increase in strength and durability [22].

Regarding the selection of the adequate surface treatment, a number of factors should be considered. For obvious reasons, the equipment and the size of the parts available during the preparation of the specimens will narrow most of the options. Then, the type of adherend and adhesive are extremely important, since the same treatment may not have the same effectiveness for different adherends using the same adhesive, and vice-versa (Table 3). Also, for some applications and in some scenarios, a more effective treatment may not be the best option, either due to its economic feasibility or the time needed and complexity of the process.

Among the different adherend materials, aluminium is one of the most common materials to be adhesively bonded, due to the widespread application of aluminium and adhesives in the transportation industry. Finding the proper surface treatment for aluminium and studying its influence in the durability of the joints has been a major concern for researchers. A thorough review on the different surface treatments for aluminium, combining several papers and studies regarding their effect on the durability of the bonds has been done by Critchlow et al. [31].

Table 3 - Effect of metal substrate preparation in adhesive bonded joints for an epoxy adhesive (adapted from [9]

Adherend	**Treatment**	**Shear Strength [MPa]**
Aluminium	As received	3.06
Aluminium	Degreasing	5.77
Aluminium	Mechanical	12.
Aluminium	Chemical	19.0
Titanium	Acid etch	21.8
Titanium	Liquid pickle	22.9
Titanium	Liquid hone	26.9
Titanium	Hydrofluorosilicic acid etch	27.6

The most common surface treatments, mechanical treatments such as grit-blasting or sandblasting, combined with degreasing, produce a highly macro-rough surface. This treatment usually precedes a chemical or an electrochemical treatment that enhances the micro-roughness of the adherends. Usually, etching or anodizing with an acid solution is one of the most effective methods to properly prepare aluminium.

Anodizing is an electrolytic passivation process that grows an oxide layer in the surface of the adherend, by passing a current through an electrolyte solution. The part to be anodized serves as the anode, while a sacrifice metal is used as the cathode. For many years, chromic-acid anodizing (CAA) was the most preferred treatment for aluminium. However, due to the hazardous residues resultant from the anodization and the more strict regulations imposed by the European Union, this method is no longer performed [32]. Instead, the phosphoric-acid anodizing (PAA) has replaced it, with treatable residues after the anodization and an equal effectiveness [4, 30-33]. Other techniques such as sol-gel coating or laser treatments [30, 34] are more recent and

therefore do not have as much information available in terms of their performance as the classical treatments. In general, these newer technologies are far more expensive than the classic ones, and only in some cases its use is justifiable.

2.5. Strength prediction

There are three basic approaches in order to characterize adhesive joints fracture: continuum mechanics, fracture mechanics and the combination of both, damage mechanics.

2.5.1. Analytical solutions

2.5.1.1. Volkersen

Volkersen [35] developed a model that considers the elastic deformation of the adherends, while keeping the adhesive only loaded in shear, as represented in Figure 12. The differential in the strain of the adherend results in a non-linear shear stress distribution in the bonded layer, where the shear stress is maximum at the ends of the overlap and minimum in the middle.

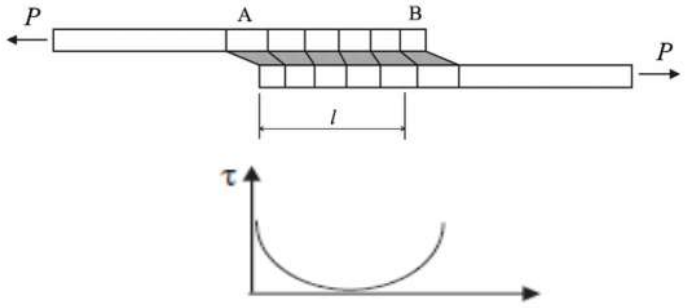

Figure 12 - Deformation and stress distribution of a SLJ according to Volkersen [36]

Because of the assumptions made, the bending moment that occurs in SLJs due to the non-collinearity of the forces applied is despised, making this method more accurate for double-lap joints (DLJ's), where this effect is not as significant as in SLJ's. Also, for composites, this method is even less accurate because of the low shear and transverse modulus of this type of materials, that aggravates the adherend bending and the shear deformations [22].

2.5.1.2. Goland and Reissner

After Volkersen's analysis, Goland and Reissner [37] proposed a different approach. They were the firsts to consider the bending moment (M) and the transverse force (V) that act in the bonded layer due to the non-collinearity of the applied load (P) in the SLJ (Figure 13). This bending moment will cause a rotation that creates a non-linear geometric problem, and the large deflections in the adherends so far negligible have to be considered.

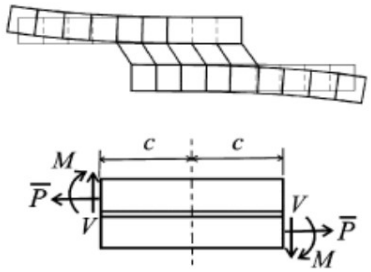

Figure 13 - Goland and Reissner's model [37]

The transverse force induces shear and peel stresses in the joint, with a stress distribution similar to the one described by Volkersen. However, this analysis results in a higher shear stress value, because it takes into account the peel stresses as well (Figure 14). The large deflections in the adherends are considered, with the adherends being integral and the adhesive layer infinitely thin.

Despite the advances made, the model did not take into account the plastic deformation of the adhesive or the shear and normal deformations in the adherends. Still, it accurately predicts the failure of brittle adhesives, and at the time made even clearer

the relevance of the bending moment in the analysis of SLJ's, and thus the need to take into consideration peel stresses [38].

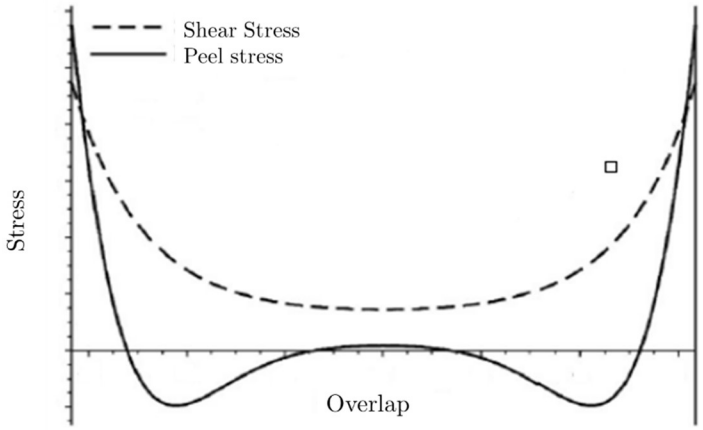

Figure 14 - Goland and Reissner's shear and peel stresses distribution along the overlap [37]

2.5.1.3. Hart-Smith

In 1973, Hart-Smith [23], considered that the adhesive not only deformed elastically but also plastically taking a step further the SLJs analysis started by Volkersen and Goland and Reissner (Figure 15). For this analysis, the ultimate strength and strain of the joint is the same as the adhesive, with the strain energy of both adhesive and joint being the same. This allowed for a higher prediction than the previous model, having the maximum shear strain of the adhesive as the failure criterion [39].

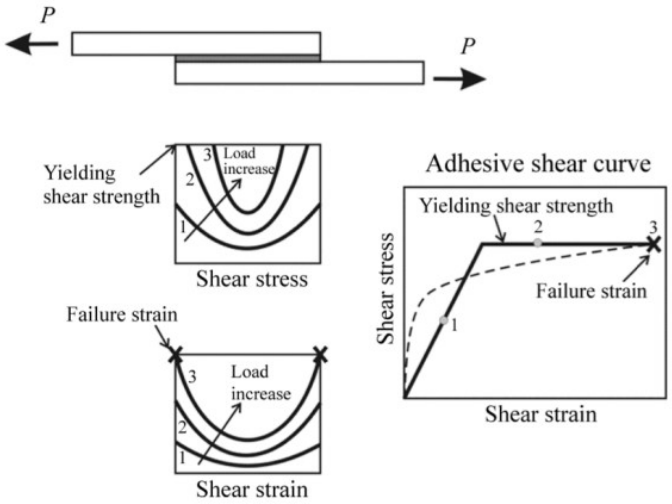

Figure 15 - Shear plasticity in the adhesive proposed by Hart-Smith [11]

2.5.1.4. Global yielding

This simple analysis was proposed by Adams et al. [21] and can predict the joint strength for ductile adhesives and adherends. If the adhesive and the adherends are brittle, the model does not apply and it is recommended to use finite element analysis to predict the failure load [21]. The methodology is shown in Figure 16.

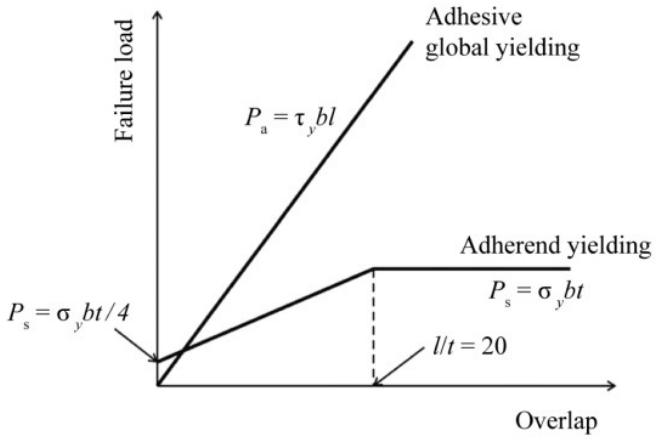

Figure 16 - Global yielding criterion for SLJs based on adherend yielding [11]

The adhesive is considered ductile if the shear failure strain is over 20%. When elastic adherends are used for the SLJ's, the failure load corresponds to the total plastic deformation of the adhesive, and the failure load P_a is:

$$P_a = \tau_y bl \quad [1]$$

Where τ_y is the yield strength of the adhesive, b the width of the joint and l the length of the overlap. If the adherends are ductile the failure load of the joint tends to a certain value with an increase in the overlap, which corresponds to the yielding of the adherend. For this case, the direct tensile stress (σ_t) acting in the adherend and caused by the load P is given by:

$$\sigma_t = \frac{P}{bt} \quad [2]$$

With t being the thickness of the adherend. If we consider a bending moment (M) following Goland and Reissner's approach, the stress applied to the adherend's surface (σ_s) comes:

$$\sigma_s = \frac{6M}{bt^2} \quad [40]$$

Where $M = \frac{kPt}{2}$ [37]. k is a bending factor which starts at unity and decreases with the rotation of the lap joint under load. The real stress acting in the adherend is in fact a combination between the direct stress and the bending stress. Considering this, the maximum load allowed P_s is:

$$P_s = \frac{\sigma_y bt}{(1+3k)} \quad [4]$$

Where σ_y is the yield strength of the adherend. If the joint in study has a short overlap or is subjected to a relatively small load, the value of k can be considered 1. Therefore, rearranging Equation 4:

$$P_s = \frac{\sigma_y bt}{4} \quad [5]$$

If the relation between the overlap length and thickness of the adhesive is over 20 ($\frac{l}{t} \geq 20$), the value of k will eventually reach 0, meaning that the bonded area yields. For this case the joint strength is then given by:

$$P_y = \sigma_y bt \quad [6]$$

2.5.2. Numerical approach

SLJ's behaviour can be governed by relatively simple equations. However, the analysis of adhesive joints can be highly complex if composite adherends are used, the adhesive deforms plastically or if there is an adhesive fillet [41]. For these cases, a numerical method is more adequate to properly predict the strength of the joints. This prediction requires previous knowledge of the adhesive and adherends properties that describe the mechanical behaviour of the materials, such as strength and energy parameters, hence the need of the different tests performed with the adhesive in this project.

The numerical approach follows damage mechanics, which are a combination of both continuum and fracture mechanics. Continuum mechanics use the maximum values of stress and strain predicted by FEA and then compare them with the material properties, assuming that the bond between the adhesive and the adherends is perfect. The predictions of stress and strain using this approach are much dependent on the singularity points existent at the corners of the adherends, because they increase the values of the predictions [42]. Fracture mechanics are only valid under elastic deformations, assuming that the structure is a non-continuous body. In this case, defects such as delamination, debonding or cracks are points of stress concentration that are likely to be points of fracture, causing the failure of the component [43]. This failure is determined once the strength of the material is surpassed for a relative displacement.

By applying these two philosophies, it is possible to model the behaviour of the adhesives using a cohesive zone model (CZM). The fracture is considered to be a gradual phenomenon in which the separation law takes place across an extended crack "tip", or cohesive zone, and is opposed by cohesive traction [44] The cohesive zone elements (CZE) represent the forces existent between the material layers, and the damage evolution of this elements is governed by traction separation laws. These laws rule the behaviour of the material under pure mode loads (mode I, II), assuming that the energy is dissipated as the crack grows, and that area is determined by the area under a stress displacement curve [45, 46]. There are two major types of cohesive laws (Figure 17).

-trapezoidal cohesive law: it best represents the behaviour of materials, especially those with a significant ductility.

-triangular cohesive law: this law is most adequate for brittle materials that do not show a ductile behaviour. It is also much easier to implement when in comparison with the trapezoidal law.

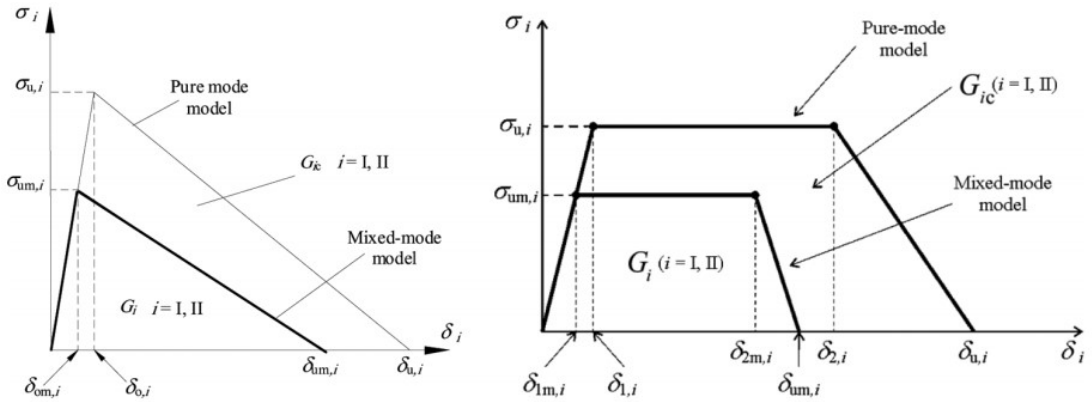

Figure 17 - Different traction separation laws [43]

For the first part of the curve a linear elastic behaviour is assumed, followed by either a linear softening or a plateau before the softening initiates, depending on the type of cohesive law. To characterize these laws, the stiffness and strength of the material under mode I and mode II solicitations are required, as well as the fracture energy in mode I and II (the latter parameters are obtain by performing fracture tests, further described in Section 2.8). These last two parameters, defined by the area under the stress-displacement curve, are used to calculate the maximum displacement at failure. During this project, a triangular separation law was used for every CZM.

2.6. Fracture mechanics tests

Fracture mechanics tests are often the best solution to determine the fracture toughness of adhesives in different loads. Fracture toughness (or fracture energy) effectively measures the dissipated energy during the crack growth until fracture. A lower value corresponds to a brittle fracture, while a higher value indicates a ductile fracture. The type of fracture is different accordingly to the load applied of the adhesive, i.e. mode I, mode II or mixed mode.

After the test is performed, a data reduction scheme is required to derive the fracture toughness from the load-displacement results recorded during the test. This type of techniques rely on linear elastic fracture mechanics (LEFM) principles, with the most common ones being the compliance calibration method (CCM), the direct beam theory (DBT) and the corrected beam theory (CBT), that depend on crack measurement during propagation. More recently, Moura et al. [47] developed a new technique, the compliance-based beam theory (CBBM), that allows the determination of the fracture energy without the need to monitor the crack length during propagation. This is possible by assessing the specimen's compliance (displacement divided by the applied load) during the test, thus accounting for shear, localized plasticization and bending rotation effects [48]. The equivalent crack length, a_{eq}, that derives the crack location is then calculated based only in the compliance of the specimen, and takes into consideration the fracture process zone (FPZ) effects at the crack tip (Figure 18) [47]. This method is both applicable to the mode I and mode II fracture tests [47, 49, 50].

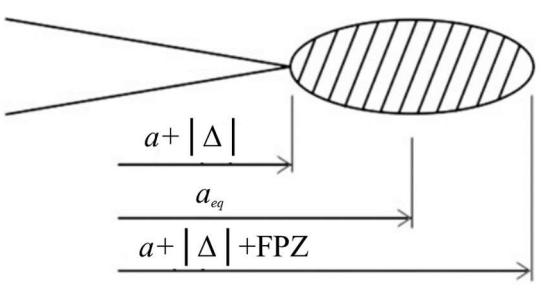

Figure 18 – Schematic representation of the FPZ and crack equivalent concept [47]

2.6.1. Mode I – DCB

The double cantilever beam (DCB) and the tapered double cantilever beam (TDCB) are the most used tests to determine the fracture toughness in mode I, with the main difference between them being the geometry of the specimens. For this project the DCB test was chosen, with the specimen's preparation and the test parameters used described in sections 3.4.4 and 4.1.3, respectively. In this test, the specimen is loaded by opening the beams until failure occurs (Figure 19). The load and the displacement are recorded during the test, and analysed using a data reduction scheme.

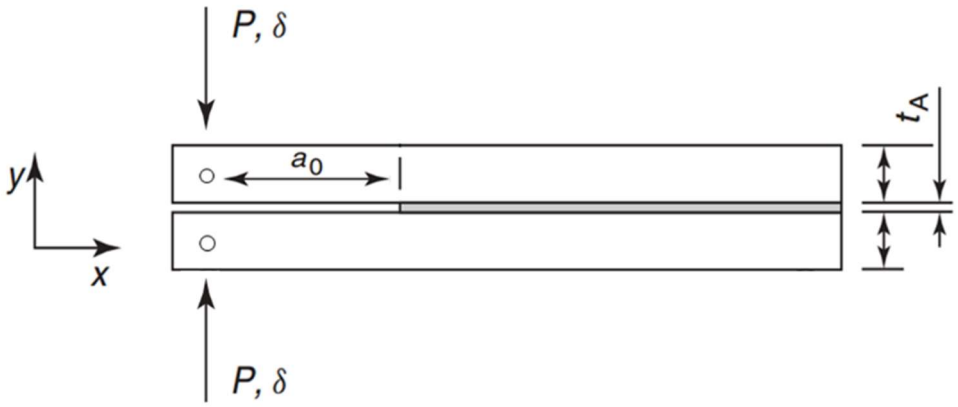

Figure 19 - DCB test setup

Using the CBBM; the fracture energy in mode I is given by:

$$G_{Ic} = \frac{6P^2}{B^2 h}\left(\frac{2{a_{eq}}^2}{h^2 E_f} + \frac{1}{5G}\right) \quad [7]$$

Where the E_f is the corrected flexural modulus to account for stress concentrations at the crack tip and stiffness variability between specimens. This modulus is obtained from the specimen's initial compliance.

2.6.2. Mode II – ENF

The end-notched flexure (ENF) and the 4-point end-notched flexure (4ENF) tests are the most commonly used to determine the fracture energy in mode II. The ENF test is a simple three point flexure test on a pre-cracked specimen, with the load applied at midlength (Figure 20), and it is the most frequently used test for mode II. The 4ENF test differs from the ENF with the load being applied by two loading cylinders, and the crack propagation appears between this cylinders. This test, despite having a more stable crack propagation than the ENF, has less information available regarding the method, and demands a more complex setup [48].

For this project the ENF test was chosen, with the specimen's preparation and the test parameters used described in sections 3.4.4 and 4.1.4, respectively. In this test, the relative displacement between the specimens introduces a mode II load in the adhesive layer, until the crack has propagated completely. The load and the displacement are recorded during the test, and analysed using a data reduction scheme.

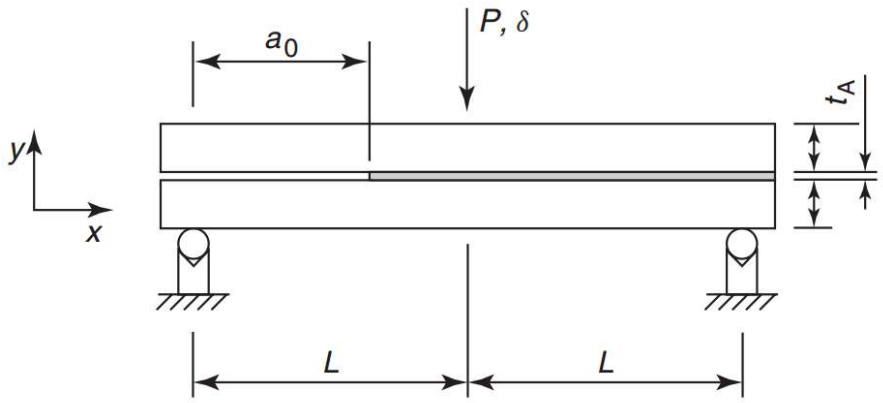

Figure 20 - ENF test setup

Using the CBBM, the fracture energy in mode II is given by:

$$G_{IIc} = \frac{9P^2 {a_{eq}}^2}{16B^2 E_f h^3} \quad [8]$$

3. Experimental details

3.1. Adhesive

The adhesive used in this thesis was the AF 163-2K, with 25.28 kg/m^2 of weight per area (nominal weight of 0.06 lb/ft^2 accordingly to the manufacturer), supplied by 3M Scotch-Weld. This is a modified epoxy structural adhesive with a knit supporting carrier, whose main function is to ensure the thickness of the adhesive layer. This adhesive has been most used in the aeronautical and aerospace industries [33, 51].

The cure cycle of this adhesive is shown in Figure 21, and these parameters were kept for every specimen and SLJ during this thesis [40]. Because it was necessary to know the cohesive laws of the adhesive to accurately simulate its behaviour, it was mandatory to determine the fracture toughness in pure modes I and II, as well as the stiffness, tensile strength and the shear strength of the adhesive. In order to fully characterize the adhesive, Bulk Tensile Testing (tensile strength, stiffness), DCB (fracture energy in pure mode I), ENF (fracture energy in pure mode II) and Thick Adherend Shear Test (TAST, shear strength) tests were performed.

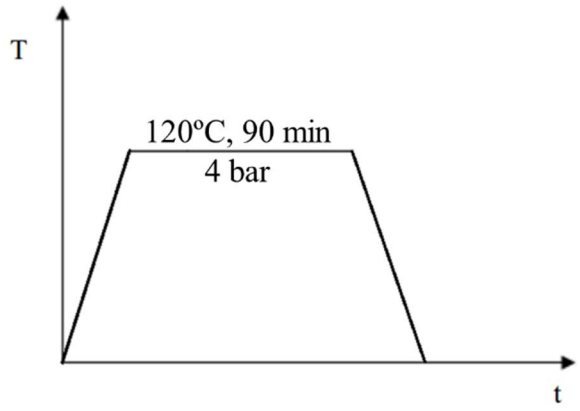

Figure 21 - Cure cycle for the adhesive AF 163-2K

3.2. Adherends

The main objective of this work was to improve the peel strength of the CFRP-only composite using aluminium in a concept similar to FML, organized differently in order to assess the best configuration in terms of mechanical properties.

The thickness of every laminate was pre-defined, 3.2 mm. This thickness was chosen because of the availability of the aluminium sheets, to allow different combinations. The ratio in volume between CFRP and the metallic alloy is also defined for every FML, 3:1 (75% of CFRP to 25% of metal). The number of configurations used was dependent on the stock availability of the metallic sheets, and also taking into consideration the time and resources necessaries to produce the laminates.

3.2.1. CFRP

The CFRP used in this study was a unidirectional 0º carbon-epoxy composite, HS 160 T700, supplied in 300 mm x 300 mm sheets of pre-preg layers by Composite Materials, Italy. The laminates were manufactured using a manual lay-up method, further described in 3.4.1, and the cure was performed in a hot plates press (Figure 22).

Figure 22 - Hot plates press machine, INTOCO

The material properties of the CFRP, considered an orthotropic material, were determined previously by Campilho [52], and are presented in Table 4.

Table 4 - Orthotropic components for a unidirectional CFRP ply [52]

E_x [MPa]	E_y [MPa]	E_z [MPa]	υ_{zy}	υ_{yz}	υ_{xz}	G_{xy} [MPa]	G_{yz} [MPa]	G_{xz} [MPa]
109000	8819	8819	0.342	0.342	0.38	4315	4315	3200

3.2.2. Aluminium

The aluminium alloy that was chosen was the 2024-T3 Alclad, with copper being the main alloying metal. This specific alloy has been used extensively in the aviation industry and in fibre metal laminates, namely the GLARE and ARALL laminates [4, 33, 53, 54]. The aluminium in question was supplied in sheets with the dimensions of 300 mm x 300 mm, with two different thicknesses: 0.8 mm and 0.4 mm, and was provided by AMI Metals, Belgium. The mechanical properties of this alloy are presented in Table 5.

Table 5 - Mechanical properties of Al-2024-T3 Alclad [55]

Young's Modulus (GPa)	**Yield Stress Strength (MPa)**	**Poisson's ratio**	**Elongation [%]**	**CTE [m/m K^{-1}]**
66	350	0.33	12	23.22

3.3. FML configuration

The number of configurations used was dependent on the stock availability of the metallic sheets and their thicknesses, and the time and resources necessaries to produce the laminates. During the project, aluminium with 0.4 mm and 0.8mm were available.

Taking also into consideration the fact that the thickness of the CFRP layers is limited by the thickness of the pre-preg layer, and for the sake of an easier and not very time-consuming manufacture, the configurations chosen are presented in Figure 23.

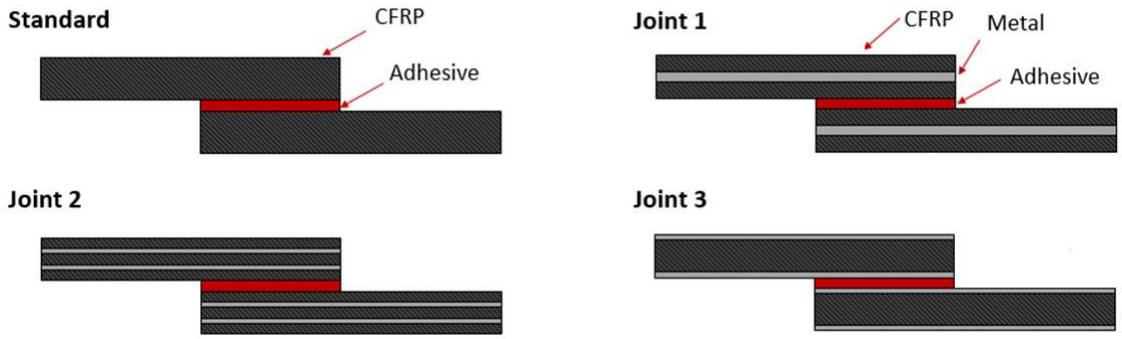

Figure 23 - Selected configurations for FML

In the beginning of the project, the initial plan was to use both aluminium and titanium to manufacture the FML in order to study the joint strength behaviour of the FML using different materials. The idea was to use one of the most common type of titanium alloys in the aircraft industry, the alpha-beta Ti-6Al-4V. However, and despite the availability of this material in sheets with 0.8 mm thickness, it was not possible to cut the sheets into the desired shapes without damaging both the plate and the cutting tools, due to the high strength of this material.

3.4. Specimens manufacture

3.4.1. CFRP plates

The manufacturing process of a CFRP plate has the following procedure:

1. Defrost the pre-preg layers necessary for the desired thickness (each layer has 0.15 mm of thickness) until it reaches room temperature.
2. Clean and degrease (with acetone) the mould sheets and the spacers. After this it is necessary to apply a mould releasing agent in order to ease the removal process after the cure (during this project, the Loctite® Frekote 770-NC,

manufactured by Henkel was the mould releasing agent chosen, since it usually works well for most epoxy-based adhesives [48]). Three coats of this product were applied.

Figure 24 - Drying of the mould releasing agent

3. Manually stack the pre-preg layers, with attention to the direction of the fibres. Each layer is covered with Teflon on one side and paper on the other. Two layers are disposed side by side, and are subsequently heated for a short period of time using a hot air gun (the amount necessary to facilitate the adhesion between the layers, but without starting the cure process), Figure 25. In order to ensure a thickness of 3.2 mm, and considering that the thickness of each prepreg layer is 0.15 mm, 21 plies were stacked, and the final thickness was assured by spacers of the mould.

Figure 25 - Pre heating of the CFRP pre-preg layers

4. After bonding them, pressure is applied with a scraper to avoid air bubbles and ensure a good adhesion, and the paper coating is removed in order to place the next layer.

5. After all the layers are put together, it is advised to cool the plate until it reaches room temperature, and only then begin the curing process. The plate is then cured accordingly to the supplier recommendations: a heating rate of 4ºC/min until it reaches 130ºC, and then it is kept under this temperature for an hour, while being under a pressure of 30 bar. After that it is cooled under pressure until it reaches room temperature.

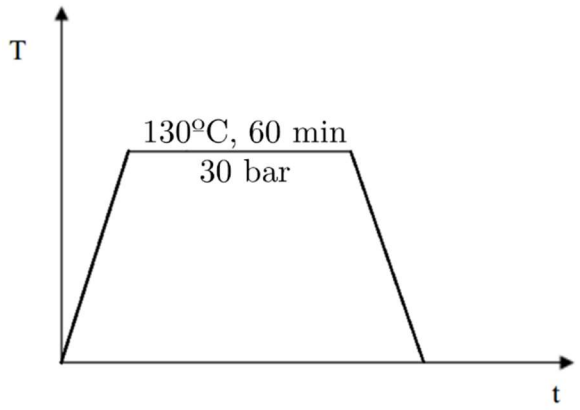

Figure 26 - Cure cycle for the CFRP plates

6. After curing the plate is then cut into the desired shape using a specific tool (conventional tools wear out quicker when cutting carbon fibre), in this case a diamond disc cutting machine (model DV 25 Batisti Meccanica, Italy). The thickness of the plate is also measured at the end of the cure to confirm the desired value.

3.4.2. Bulk test specimens

The manufacturing process for producing bulk adhesive specimens for tensile testing was as follows:

1. Defrost the role of adhesive until it reaches room temperature. It is not advised to use the adhesive right after being taken from the freezer.
2. Cut a silicone shape that will stand between the adhesive and the mould walls. This will stop the adhesive from leaking and will force the adhesive to cure within the desired shape, thus avoiding air bubbles and other defects.

3. Cut 9 layers of adhesive to fabricate the adhesive sheet. Each layer has 0.2413 mm of thickness (9.5 mils), and 9 layers were used, with the final thickness of the bulk plate (2 mm) being ensured using spacers between the mould base and the mould lid (Figure 27) [48].

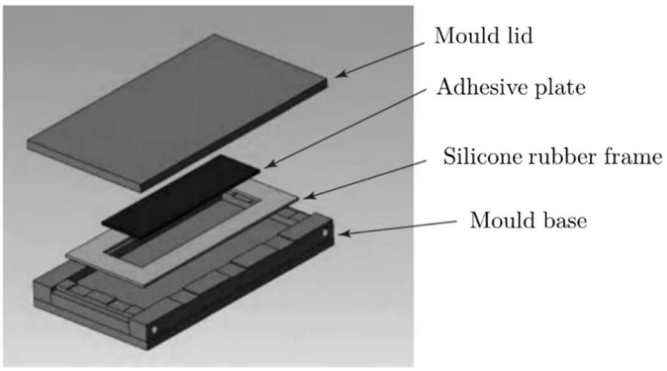

Figure 27 - Schematic view of the mould and the silicone rubber frame [48]

4. Clean and degrease (with acetone) the mould sheets and the spacers. After this it is necessary to apply a mould releasing agent in order to ease the removal process after the cure. Three coats of this product were applied.
5. Manually stack the adhesive film layers. Each layer is covered with Teflon on one side and paper on the other. After bonding them pressure is applied with a scraper to avoid air bubbles and guarantee a good adhesion, and the paper coating is removed in order to place the next layer (Figure 28).

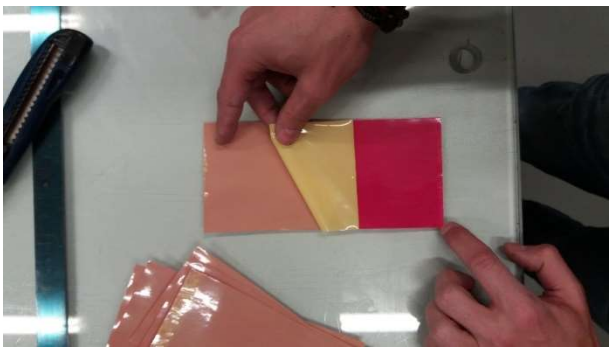

Figure 28 - Removal of the protective Teflon layers of the adhesive film

6. After all the layers are put together, the cover papers from the bottom and the top layers are removed and the layup is then inserted into the mould with the silicone rubber frame.

Figure 29 - Mould with silicone rubber frame and the bulk adhesive

7. The curing process follows the curing cycle recommended by the material supplier, and is carried in a hot plates press. First the adhesive is gradually heated with a slope of 4ºC/min, until it reaches 120ºC, and then is kept under this temperature for 90 min, while being under a pressure of 4 bar. After this time the bulk plate is then cooled under pressure until it reaches room temperature.

Figure 30 - Mould inserted into the hot plates press

8. Once the plate is cooled it is then machined into the bulk specimens with the normalized dimensions, accordingly to the standard NF T 76-142 (Figure 31) [56]. The thickness of the plate is also measured at the end of the cure to confirm the desired value.

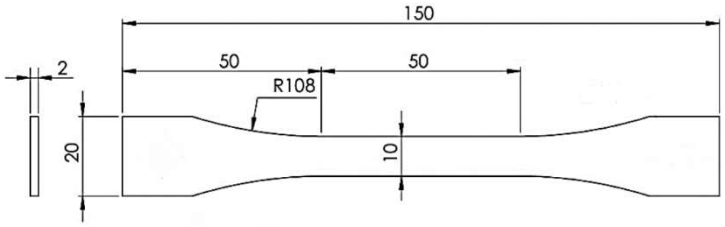

Figure 31 - Bulk specimen geometry (dimensions in mm)

3.4.3. TAST specimens

The manufacturing process for producing specimens for TAST testing was as follows:

1. Sandblast the specimens and then degrease them with acetone in order to assure a strong bond. Usually the adherends are made of steel, since it reduces the adherend deformation and rotation when in comparison with an aluminium specimen. The specimen's dimensions follow the ISO 11003-2 (Figure 32) [57].

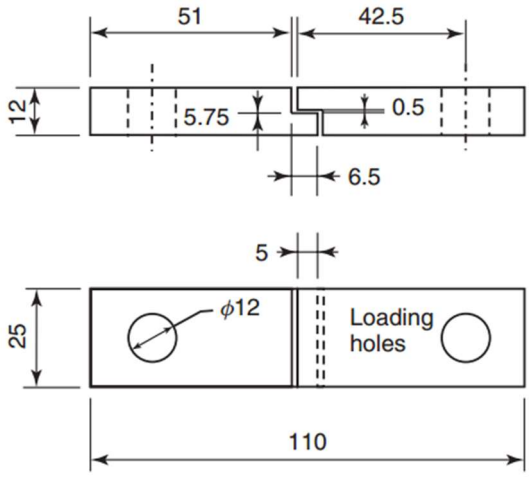

Figure 32 - TAST specimen geometry (dimensions in millimetres)

2. Apply a mould releasing agent in the mould and in the shims that will be placed between the adherends in order to ensure the overlap length (Figure 33).

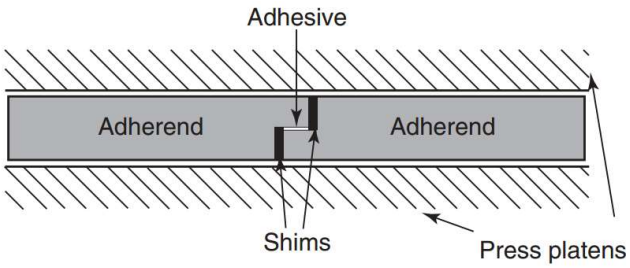

Figure 33 - Schematic view of the mould with the TAST specimens [48]

3. Cut the adhesive with the overlap dimensions and carefully place in the right position, after the removal of the Teflon and the paper protections. If by any

means the adhesive contacts any unprepared surface the process should be repeated and a new piece of adhesive cut.

4. The curing follows the parameters mentioned for the bulk specimens.
5. After the cure process the shims are removed and the excess of adhesive is removed using a file or sand paper. The dimensions of both the thickness of the adhesive and the thickness of the adherends are measured, since the specimens are reutilized and the original dimensions may not be the actual ones.

3.4.4. DCB and ENF specimens

The DCB and the ENF tests use the same type of specimens, which geometry is presented in Figure 34, following the ASTM D3433-99 [58].

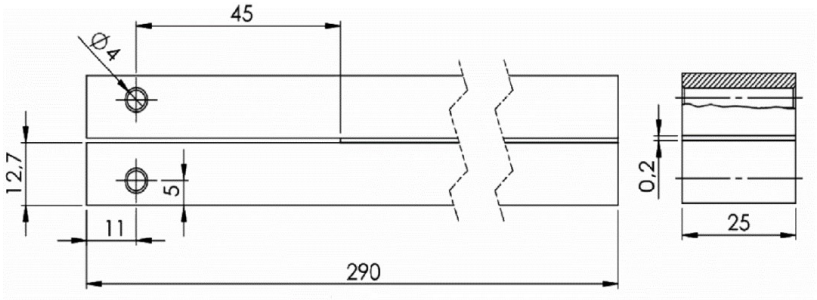

Figure 34 - DCB and ENF specimen's geometry (dimensions in millimetres)

The manufacturing process of this specimens has the following procedure:

1. Roughening the surface of the steel specimens by grit blasting, preceded and followed by degreasing with acetone.
2. In order to assure the thickness of the adhesive, and despite the fact that the adhesive in study was knit supported, at both ends of the bonding length calibrated steel spacers were placed. These spacers have a blade in the middle to induce a pre-crack in the adhesive layer. Three coats of a mould releasing agent are applied to this spacers for an easy removal.

3. The cure of the adhesive followed the parameters previously mentioned, as well as the preparation of the mould.
4. After the cure the excess of the adhesive on the lateral sides of the specimens must be removed so that the crack in the adhesive layer can be easily identified.
5. Before both DCB and ENF tests, a pre-crack is produced by loading the specimens for a short period of time before the actual test. This prevents the effect of blunt crack and ensure the right propagation of the crack. Only after this loading the initial crack length is measured.

The adhesive thickness has a major importance during this test, since it influences the mechanical properties. This is due to the varying degree of constraint to deformations around the crack tip, which will naturally affect the way FPZ is propagated [50].

3.4.5. FML

The manufacture of the FML follows the same principle as the manufacture of the CFRP plates. However, and accordingly to the type of configuration of the FML, the CFRP is interleaved with aluminium sheets. The manufacture procedure of a CFRP-Al-CFRP plate was as follows:

1. Stack two different laminates of CFRP (without curing them) following the procedure described previously, with the desired thicknesses for the FML.
2. Roughening the surface using a high granulometry sand paper, and degrease the sheets before and after the roughening using acetone.
3. Anodize the sheets following the procedure described in 3.4.6.
4. After the anodizing, remove the paper protection from the CFRP pile ups and carefully place the sheets in the desired position (Figure 35). The CFRP plates should be lightly heated using a hot air gun before the aluminium sheets are stacked.

Figure 35 - Stacking of the aluminium sheets over the CFRP laminate

5. Stack the other CFRP plate on top of the aluminium sheets to complete the FML configuration.
6. The cure of the FML plate follows the parameters previously mentioned for the CFRP, and also the preparation of the mould.
7. After curing the plate is then cut into the desired shape using a specific tool (the conventional tools wear out quicker when cutting carbon fibre).

For the other FML configurations the only difference is the number of CFRP laminates needed before the stacking of the aluminium and their thicknesses.

3.4.6. Anodizing of aluminium sheets

As established previously, in order to ensure a strong bond between aluminium and either adhesive or composites, a surface treatment more effective than sand abrasion and degreasing is required. For this project, phosphoric acid anodizing (PAA) was chosen to improve the bond strength when one of the adherends is aluminium.

The procedure followed the standard ASTM D3933-98 [59]. The setup chosen was a multi-rack system with two aluminium wires serving as cathodes (one on each side of the plate) and the plate working as the anode in the circuit, held in the electrolyte bath via two aluminium wires (Figure 36).

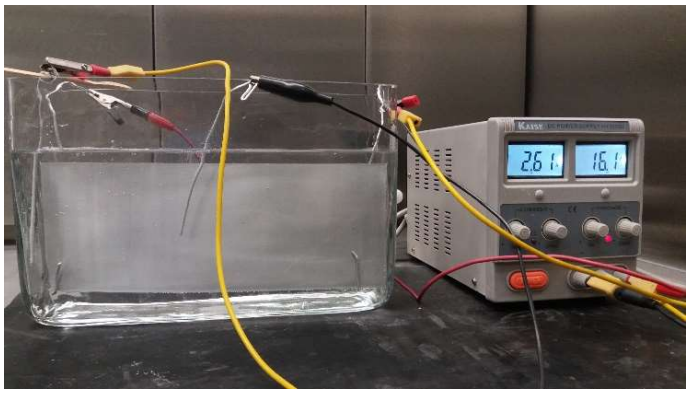

Figure 36 - Setup mounted to anodize the aluminium sheets

The voltage was fixed at 16 V for 25 minutes, with special attention regarding the temperature of the electrolyte. If the temperature rises up to 40ºC, there is a risk of burning the oxide layer formed during the anodizing process, and the process has to be redone. The whole process is composed of the following steps:

1. Cleaning the aluminium sheets by first applying a grit sandpaper, followed by degreasing the surface using acetone.
2. Prepare a solution of electrolyte with 12 wt % of H_3PO_4 (phosphoric acid), diluted in distilled water.
3. Pour the electrolyte into a glass recipient, and connect the aluminium wires that will serve as cathode to the negative pole of the supply, and submerge the aluminium sheet held by two different aluminium wires and connect them to the positive pole of the supply.
4. After verifying that the wires are not in contact with each other, turn on the power supply to 16 V, for 25 min.
5. During the anodizing process, it is advised to check the temperature and the value of the current. If the values are too high, the process should be stopped and started over.
6. After 25 minutes, turn off the power, and rinse the aluminium sheet in tap water. Then, clean the specimen with acetone and visually inspect it for burnt areas.

7. Carefully cover the aluminium sheet in aluminium foil until it is stacked with CFRP. It is not recommended to wait more than one day between the anodizing and the FML manufacture.
8. Pour the electrolyte into an appropriate container to be properly treated without any damage do the environment. After anodizing the electrolyte should be renewed to prevent overheating.

3.4.7. SLJ

The geometry chosen for the SLJ is shown in Figure 37. The distance between the edges of the overlap and the alignment tab was kept the same for the two different overlaps chosen, 12.5 and 50 mm. The width and thickness of the specimens was the same, as well as the thickness of the adhesive layer. Spacers with the same thickness of the substrate should be used to ensure the distance between the overlap and the alignment tabs.

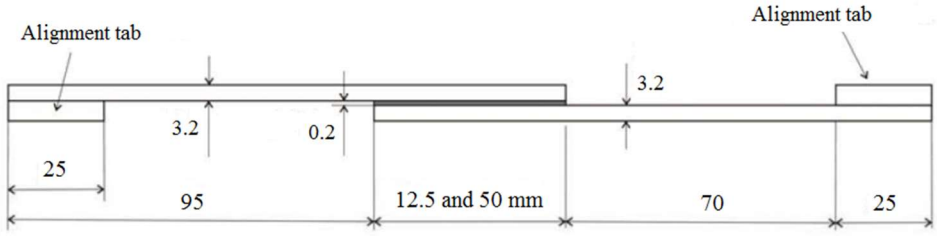

Figure 37 - SLJ geometry (dimensions in mm)

The manufacture of the SLJ joints has the following procedure:

1. After cutting the substrates and the alignment tabs, the surface is roughened using a sand paper. When the surface is aluminium, the substrate is abraded longitudinally and transversally. In the case of CFRP, the surface should be abraded in a direction angled 45° with the fibre direction. This technique is adopted with the purpose of avoid damaging the carbon fibres.
2. The specimens are then cleaned using acetone until there are no traces of carbon residues in the cloth used for the cleaning.

3. The adhesive is cut with the dimensions of the overlap and the dimensions of the alignment tab (the same adhesive is used).

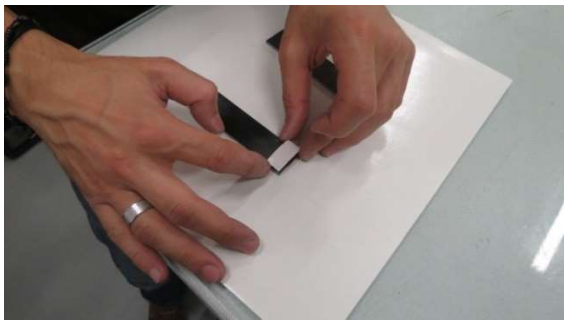

Figure 38 - Placing of the adhesive film in the adherend

4. Clean the mould to remove any particles or residues of adhesive. Then, three coats of a mould releasing agent should be applied to the mould and to the spacers.
5. Bond the alignment tabs on the end of the substrates with the adhesive. The substrates are then positioned in the mould with the spacers, and finally the top substrate is placed carefully in order to guarantee the desired overlap.

Figure 39 - Bonding of the SLJ in the mould with the spacers already in place

6. The cure of the adhesive follows the parameters previously mentioned.
7. Remove the excess of adhesive using a sand paper.
8. Drill the free end of each substrate so that a dowel pin can be inserted for gripping purposes. The holes should be drilled slowly (with special attention to the FML specimens due to the difference in the thermal expansion coefficient) and preferably using a lubricant. The surfaces should be roughened again to remove any burr from the drills.

4. Experimental results

4.1. Characterization of the adhesive

4.1.1. Tensile testing

The tensile tests for the bulk specimens were performed in an INSTRON® 3367 electro-mechanical testing machine, equipped with an INSTRON® strain gauge of 25 mm and a load cell of 30 kN, according to the standard ASTM D1002, at room temperature, with a displacement rate of 1mm/min. For fixing the specimens, two mechanical wedge-action grips were used, Figure 40. Five tests were performed, and the three most relevant test were considered. This methodology was considered for all the tests in this project.

Figure 40 - Apparatus for the bulk tensile testing

The stress-strain curves obtained from the tensile testing are presented in Figure 41. The values for the tensile strength, Young's modulus and strain failure are shown in Table 6.

Table 6 - Average values for Tensile Strength, Young's Modulus and Strain Failure

Tensile strength [MPa]	**Young's Modulus [MPa]**	**Strain failure [%]**
46.93 ± 0.63	1521.87 ± 118.29	11.00 ± 2.91

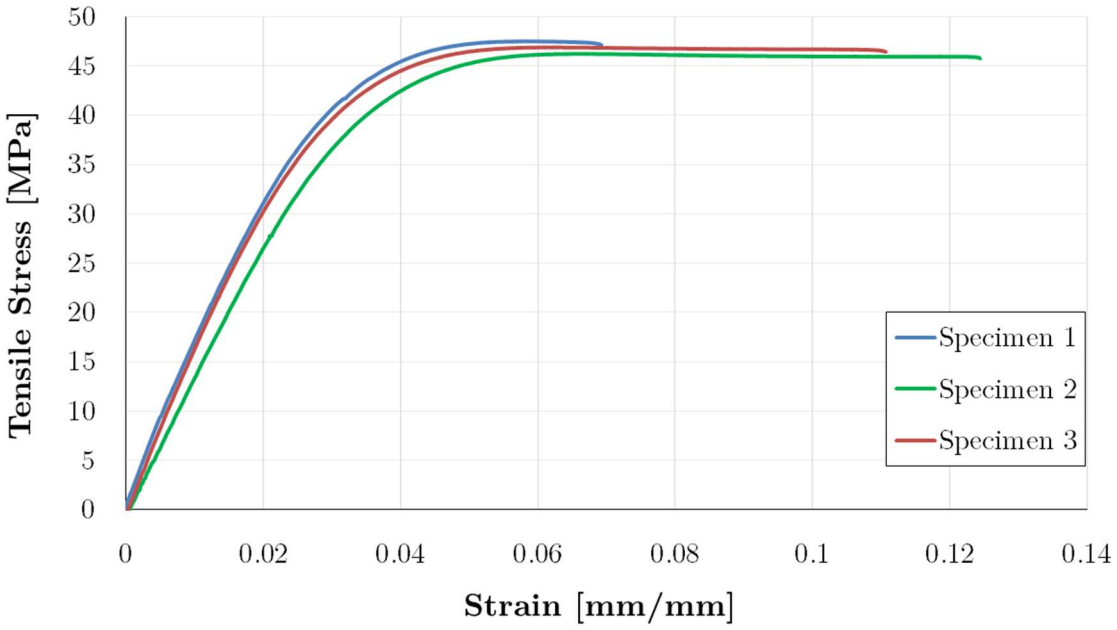

Figure 41 - Stress vs strain curves for the tensile tests

A report made by the Federal Aviation Administration studied the adhesive used in this thesis [60]. The results for both this report and the manufacturer's data are presented in Table 7. The properties obtained in this project are comparable with the ones existent in the literature. Other papers and works can be found in the literature that studied the mechanical properties of this adhesive. Work developed by Zadpoor [61] and Sargent [51] provide some base information regarding the fracture energy of this adhesive that could be used as a comparison for the experimental results that were obtained during the course of this project.

Table 7 - Results for Tensile Strength, Young's Modulus and Poisson's ratio from [60]

	Tensile Strength [MPa]	**Young's Modulus [GPa]**	**Poisson's ratio**
Manufacturer	48.30	1.11	0.34
Test results	44.10	2.53	0.37

4.1.2. TAST

The TAST test was performed in the same electro-mechanical testing machine, according to the standard ISO 11003-2. The tests occurred at room temperature, and a displacement rate of 1mm/min was used. The apparatus of test is shown in Figure 43.

Figure 42 - Apparatus for the TAST test

The values for the shear strength and shear modulus are shown in Table 8, with a fracture surface from one of the specimens in Figure 43.

Table 8 - Average values for Shear Strength and Shear Modulus

Shear strength [MPa]	**Shear Modulus [MPa]**
46.86 ± 2.57	159.73 ± 41.9

Figure 43 - Fracture surface of a TAST specimen after testing

The results obtained from the TAST tests for the shear strength were consistent. However, there was a big dispersion in the shear modulus values and in the shear strain failure ones. The TAST test effectively is not the most indicated to determine the shear modulus of an adhesive. Also, from the experimental results, and using the expression:

$$G = \frac{E}{2(1+\nu)} \quad [9]$$

The Poisson's ratio of the adhesive would be 3.76, a value unacceptable for an epoxy, normally with a Poisson's ratio between 0.3 and 0.5 [48]. Using the same expression and the Young's modulus determined experimentally, and considering a Poisson's ratio of 0.35, the shear modulus equals 563.7 MPa. This value was chosen instead of the experimental results for the numerical analysis.

Regarding the tensile strain, after an 11% tensile strain failure, which indicates a semi-ductile adhesive, it was expected for the shear strain failure to reach 30-50%. However, the maximum strain failure for the TAST was 1.7 %. This major difference in the results could be explained due to the insufficient thickness of the adhesive during the test or differences in the geometry of the specimens.

4.1.3. DCB - Mode I

The DCB test was performed with the purpose of determining the fracture energy in mode I. In order to do so, the specimens were tested by applying an opening force in one of the extremes of the specimen, Figure 44. The tests were performed electro-mechanical testing machine, at room temperature and with a displacement rate of 0.2 mm/min, accordingly to the ASTM D3433 standard. The G_{Ic} was calculated by applying the CBBM to the experimental results.

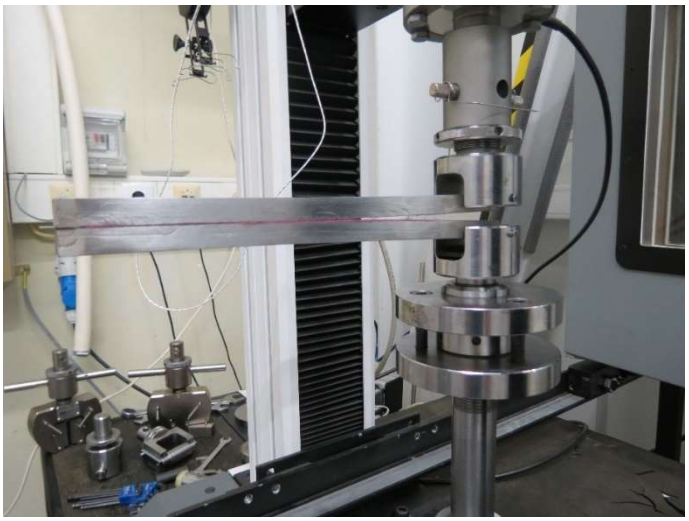

Figure 44 - Apparatus for the DCB test

The load-displacement curves obtained from the test are represented in Figure 45. The first part of the curve corresponds to the increase in the elastic energy stored, until it equals the energy necessary to propagate the crack. The crack is then propagated until the end of the bonded area; at this point the failure occurs. The R-curves resultant from the CBBM reduction are shown in Figure 46. With the crack propagation the critical strain energy converges to a plateau, corresponding to the fracture toughness of the adhesive in mode I. The value calculated for the fracture energy in mode I was 4.05 ± 0.07 N/mm.

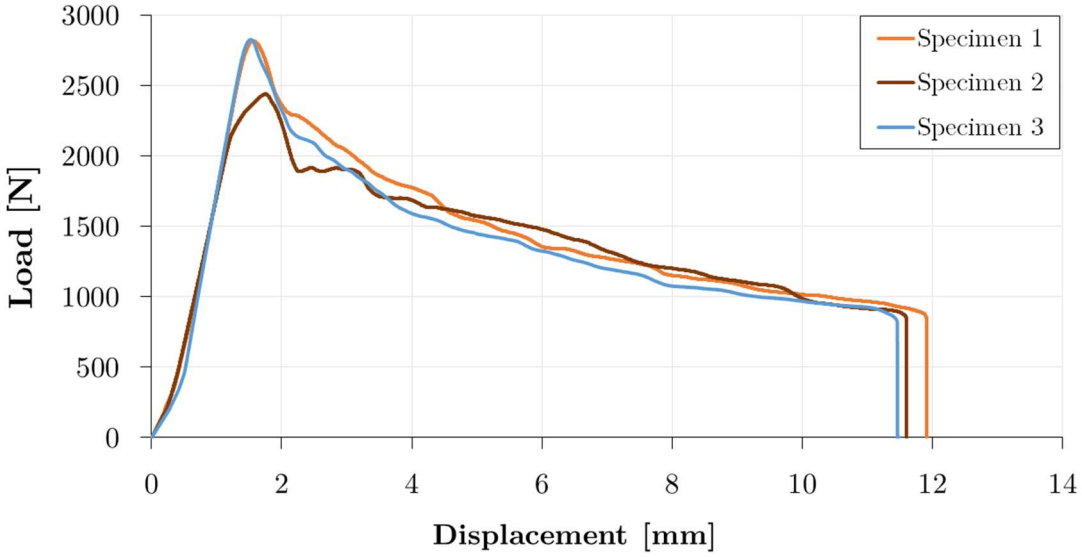

Figure 45 - Load vs displacement curves for the DCB test

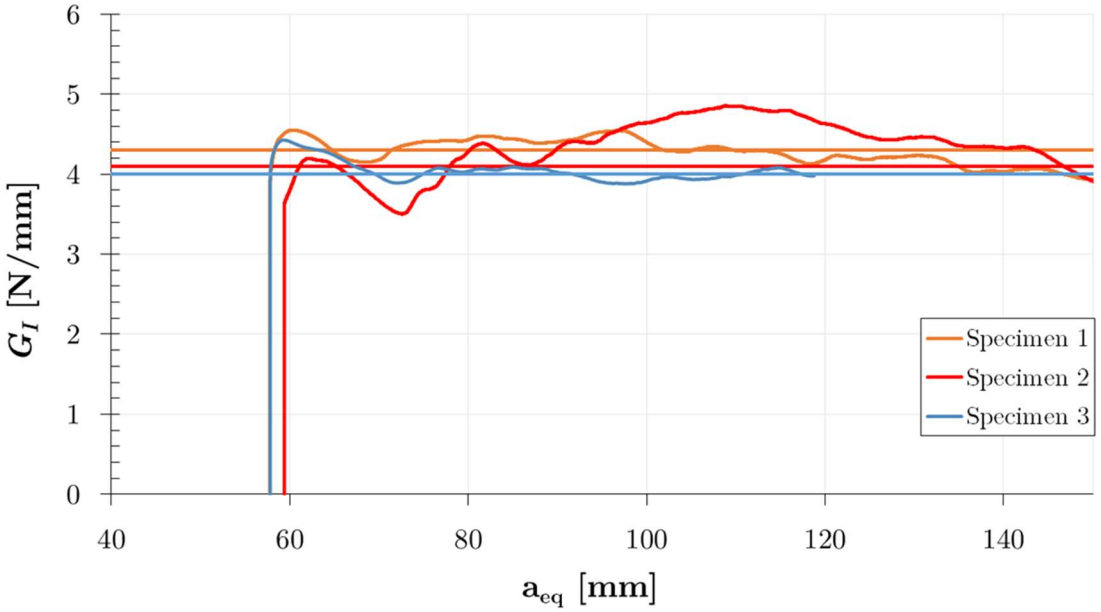

Figure 46 - Experimental R-curves obtained for the DCB test using CBBM

A typical fracture surface from the DCB test is shown in Figure 47. The failure was cohesive through the entire bonded length.

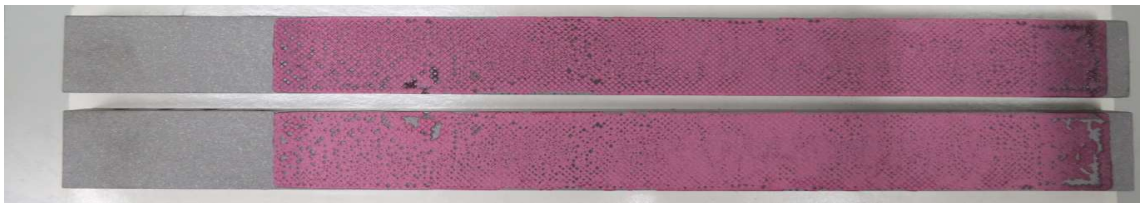

Figure 47 - Fracture surface of a specimen after the DCB test

4.1.4. ENF - Mode II

The ENF test is conducted to determine the fracture energy in mode II. The tests were performed in the same electro-mechanical testing machine, and consisted of a simple three point bending test (a simply supported beam on the extremes loaded at mid-length), with a pre-crack on one edge of the bonding length, Figure 48. After the pre-crack was done a small sheet of Teflon was introduced between the specimens where there is no adhesive, in order to ensure a frictionless contact between the specimens. All the specimens were test at room temperature and with a displacement rate of 0.2 mm/min. For adhesives, no joint geometry or apparatus have been standardized yet for the determination of the fracture energy in mode II. The G_{IIc} was obtained by applying the CBBM to the experimental results.

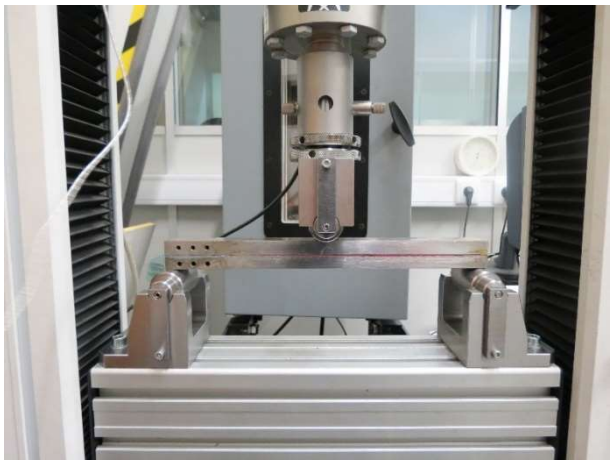

Figure 48 - Apparatus for the ENF test

The load-displacement curves obtained from the test are represented in Figure 49. The highest value for the load corresponds to the beginning of a stable crack propagation. The R-curves resultant from the CBBM reduction are shown in Figure 50. It is possible to identify a plateau in the R-curves that corresponds to the stable crack propagation during the test. By identifying this plateau it is then possible to determine the fracture toughness of the adhesive in mode II. The value calculated for the fracture energy in mode II was 9.77 ± 0.21 N/mm.

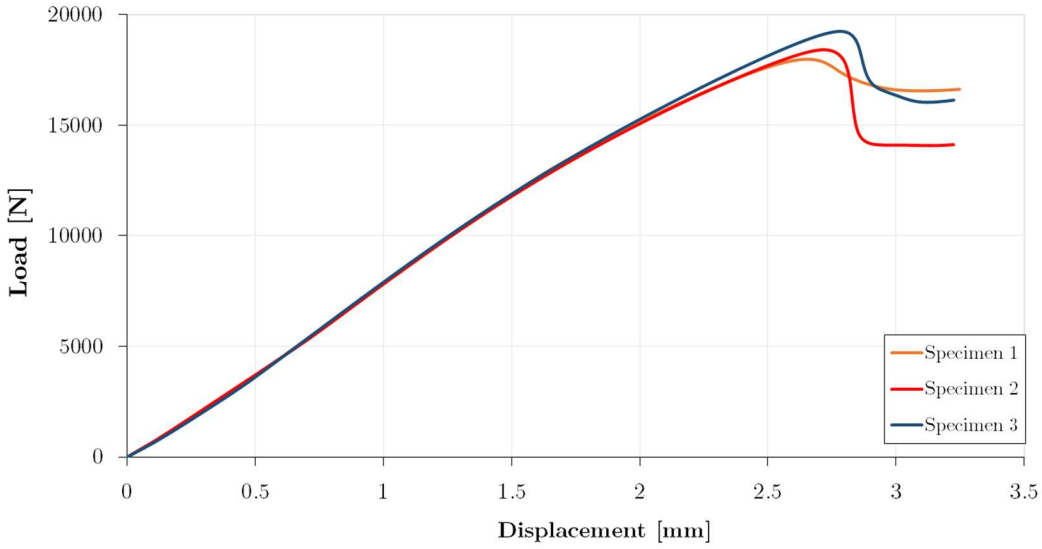

Figure 49 - Load vs displacement curves for the ENF test

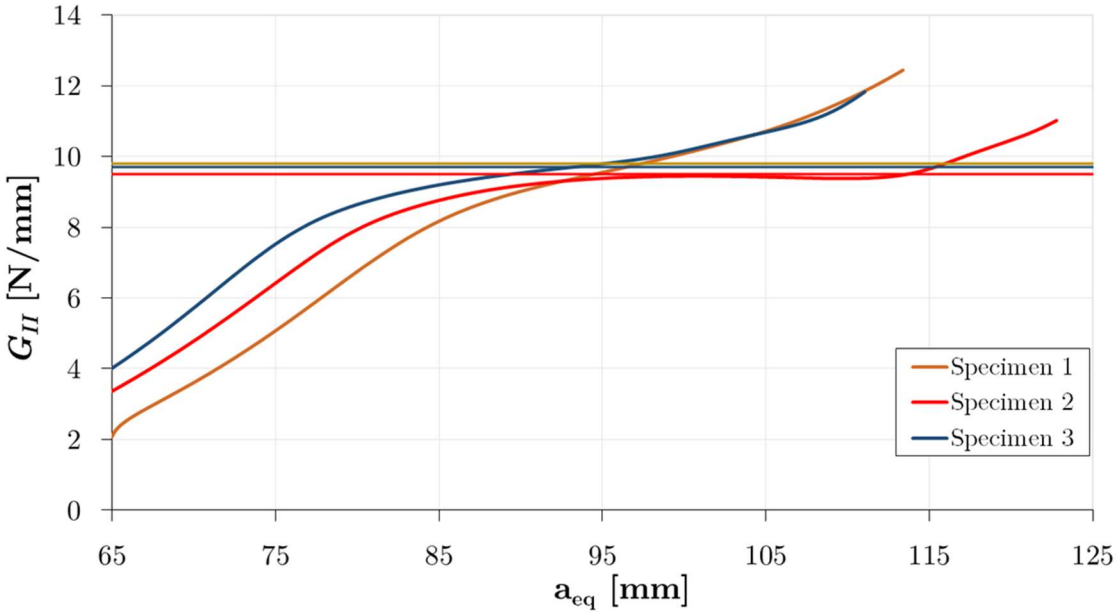

Figure 50 - Experimental R-curves obtained for the ENF test using CBBM

An example of a fracture surface from the ENF test is shown in Figure 51. The failure was cohesive in the adhesive, but close to the interface.

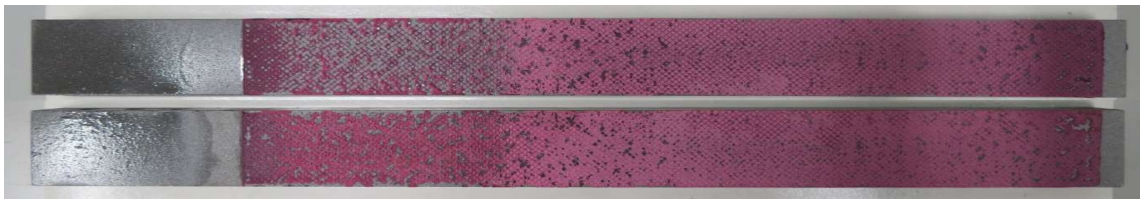

Figure 51 - Fracture surface of a specimen opened after the ENF test

A summary of the mechanical properties determined for the adhesive is presented in Table 9. This values were then used for the numerical analysis of the adhesive, characterizing both elastic and cohesive elements.

Table 9 - Summary of the mechanical properties of AF 163-2K

Tensile strength [MPa]	46.93 ± 0.63
Young's Modulus [MPa]	1521.87 ± 118.29
Shear strength [MPa]	46.86 ± 2.57
Shear Modulus* [MPa]	563.67
$\boldsymbol{G_{Ic}}$ **[N/mm]**	4.05 ± 0.07
$\boldsymbol{G_{IIc}}$ **[N/mm]**	9.77 ± 0.21

*deducted from the Young's modulus

4.2. Tensile tests of SLJ's

For the tensile testing of the SLJ's, a different machine was used, a servohydraulic model, MTS® model 810, with a load cell of 100 kN. The use of this machine was justified after testing a SLJ with CFRP-only in the Instron machine used for the previous tests. The SLJ did not fail when it reached the limit of the load cell, 30 kN, hence the need of a machine with a load cell capable of withstanding higher loads.

All the tests of the SLJ's were performed in this machine, using a different gripping system than the bulk tensile testing. The SLJ's were fixed by attaching clamps to the free extremities of the SLJ's. The alignment of the clamp with the specimen is done via a dowel pin, Figure 52. The bolts that hold the two parts of the clamp were tightened using a torque wrench and a torque of 40 N.m was applied to avoid any slippage

of the specimens during the tests. For all the FML configurations 3 specimens were tested for each overlap.

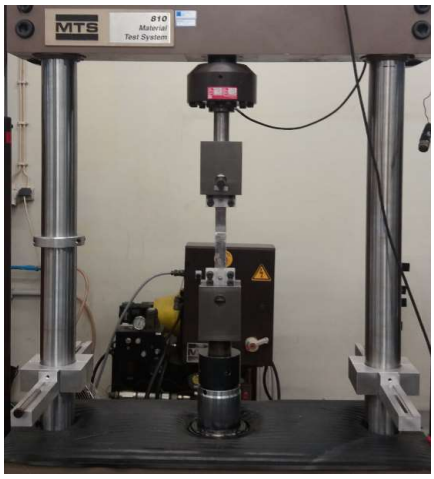

Figure 52 - Apparatus for the SLJ tensile testing

4.2.1. CFRP-Only

The purpose of this project was to assess the improvements of using different FML configurations. In order to have a benchmark to evaluate the differences between the different configurations, CFRP-only adherends were produced to serve as a reference for the other joints. The load vs displacement curves for both 12.5 mm and 50 mm overlaps are presented in Figure 53.

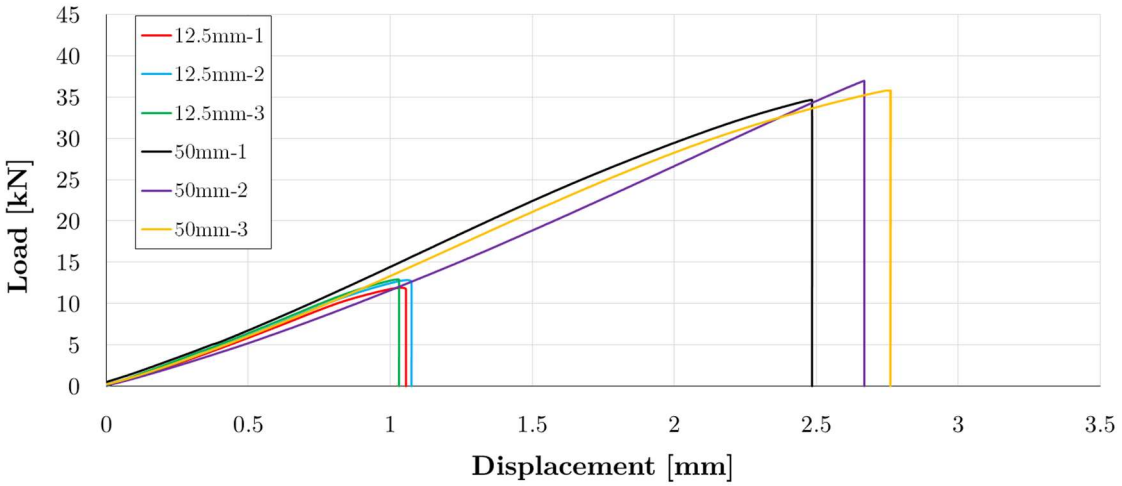

Figure 53 - Load vs displacement curves for CFRP-only specimens

Typical failure surfaces for both overlaps can be observed in Figure 54.

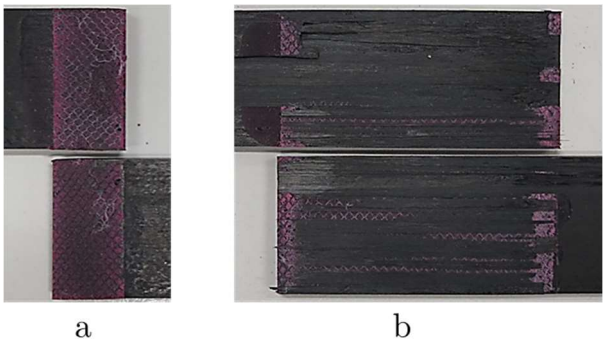

Figure 54 - Failure surfaces of SLJ with CFRP-only adherends: (a) 12.5 mm overlap; (b) 50 mm overlap

The average failure load for CFRP-only joints was 12.53 ± 0.40 kN for the 12.5 mm overlap and 37.66 ± 1.89 kN for the 50 mm overlap. For the 12.5 mm overlap the failure was cohesive in the adhesive, whereas for the 50 mm overlap there was clear delamination of the adherends. The slight difference in the slope of the curves for the 50 mm overlap and the longer displacement could be explained by a difference in the force applied to fix the clamps. A lower force would allow some slippage of the specimens, resulting in a higher strain prior to failure. Also, the standard deviation for the experimental results with 50 mm overlap may be also affected by the unpredictability of the delamination failure.

4.2.2. CFRP-Al-CFRP

The first configuration of aluminium-carbon fibre laminates consisted on CFRP reinforced with a 0.8 mm thick aluminium sheet in the middle of the adherend. The resultant load vs displacement curves can be seen in Figure 55.

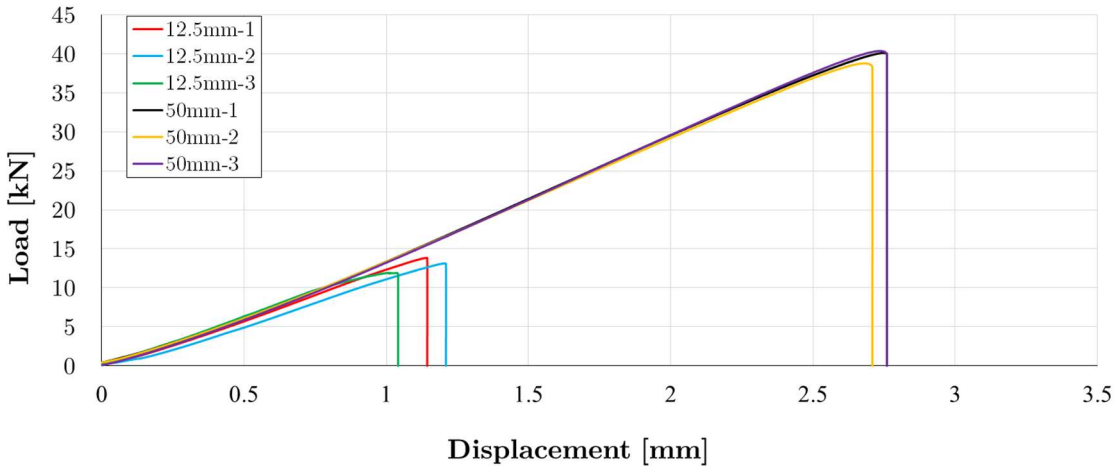

Figure 55 - Load vs displacement curves for CFRP-Al-CFRP specimens

Typical failure surfaces for both overlaps are depicted in Figure 56.

Figure 56 - Failure surfaces of SLJ with CFRP-Al-CFRP adherends (a) 12.5 mm overlap; (b) 50 mm overlap

For the CFRP-Al-CFRP configuration, the average load was 12.97 ± 0.78 kN and 39.75 ± 0.70 kN for the 12.5 mm and 50 mm overlap respectively. From Figure 56 it is possible observe a cohesive failure for the 12.5 mm overlap and delamination for the 50 mm overlap, although less severe when compared to the CFRP-only specimens.

4.2.3. CFRP-Al-CFRP-Al-CFRP

The second configuration uses two sheets of aluminium with 0.4 mm of thickness to reinforce the composite. The load vs displacement curves for both overlaps are represented in Figure 57.

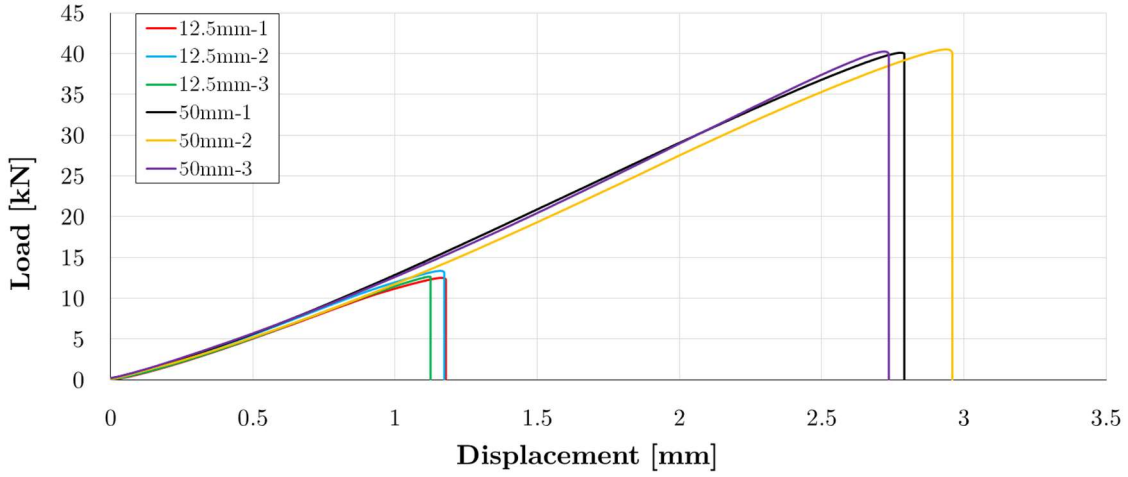

Figure 57 - Load vs displacement curves for CFRP-Al-CFRP-Al-CFRP specimens

Typical failure surfaces for both overlaps can be observed in Figure 58.

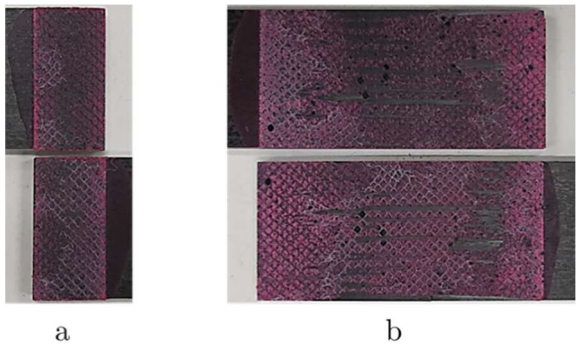

Figure 58 - Failure surfaces of SLJ with CFRP-Al-CFRP-Al-CFRP adherends (a) 12.5 mm overlap; (b) 50 mm overlap

The average failure loads was 13.00 ± 0.36 kN for the 12.5 mm overlap and 40.39 ± 0.13 kN for the 50 mm overlap. Just like the other configurations with CFRP on tops, the failure was cohesive for the 12.5 mm overlap and delamination for the 50 mm overlap.

4.2.4. Al-CFRP-Al

This configurations resembles the most the classic concept of FML. In this case the core of the laminate is CFRP, with an aluminium sheet of 0.4 mm on each top of the laminate. The load vs displacement curves for 12.5 mm and 50 mm overlap are shown in Figure 59.

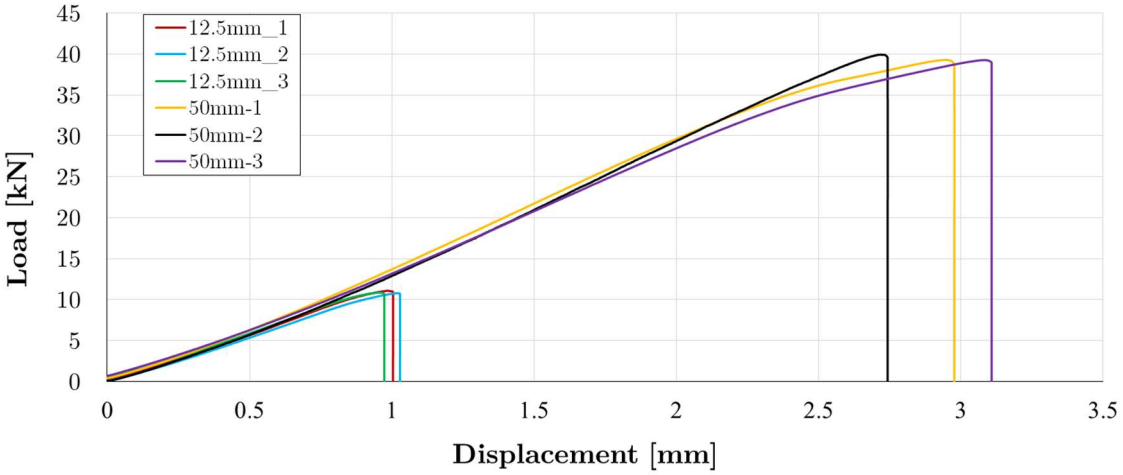

Figure 59 - Load vs displacement curves for Al-CFRP-Al specimens

Typical failure surfaces for both overlaps can be observed in Figure 60.

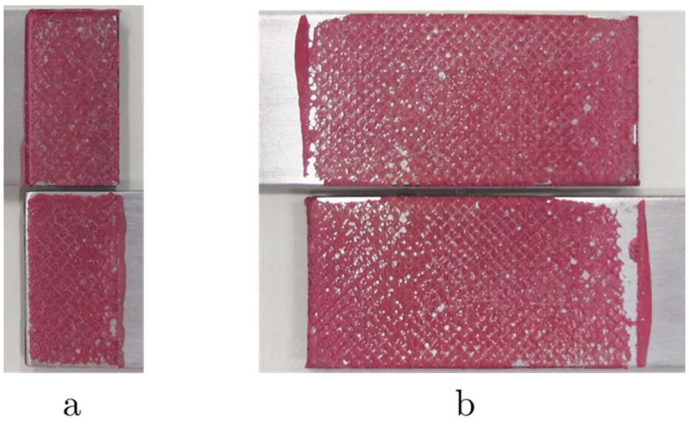

Figure 60 - Failure surfaces of SLJ with Al-CFRP-Al adherends (a) 12.5 mm overlap; (b) 50 mm overlap

The failure load for the 12.5 mm overlap was 10.91 ± 0.13 kN, and for the 50 mm overlap 39.48 ± 0.31 kN. The failure was cohesive for the 12.5 mm overlap. For the 50 mm overlap the failure was mostly cohesive, with some small areas showing an adhesive failure. For both configurations it was possible to observe some small voids in the surface, indicating that some air was trapped during the cure of the adhesive. Despite these voids and some areas of adhesive failure, the Al-CFRP-Al configuration was the only one with a cohesive failure for the 50 mm overlap.

4.3. Comparison of SLJ's results

4.3.1. SLJ's, 12.5 mm overlap

For a better comparison of the results, the failure loads, the joint strength and the type of failure for the 12.5 mm overlap are presented together in Table 10. Also, for a better understanding of the differences in the failure mode of each specimen, the failure surfaces are presented again in Figure 61.

Table 10 - Failure load and type of failure for joints with a 12.5 mm overlap

Type	**Average failure load [kN]**	**Shear joint strength [MPa]**	**Failure type**
	12.53 ± 0.40	40.10 ± 1.26	Cohesive
	12.97 ± 0.78	41.49 ± 2.51	Cohesive
	13.00 ± 0.36	41.61 ± 1.15	Cohesive
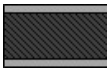	10.91 ± 0.13	34.90 ± 0.42	Cohesive + Adhesive

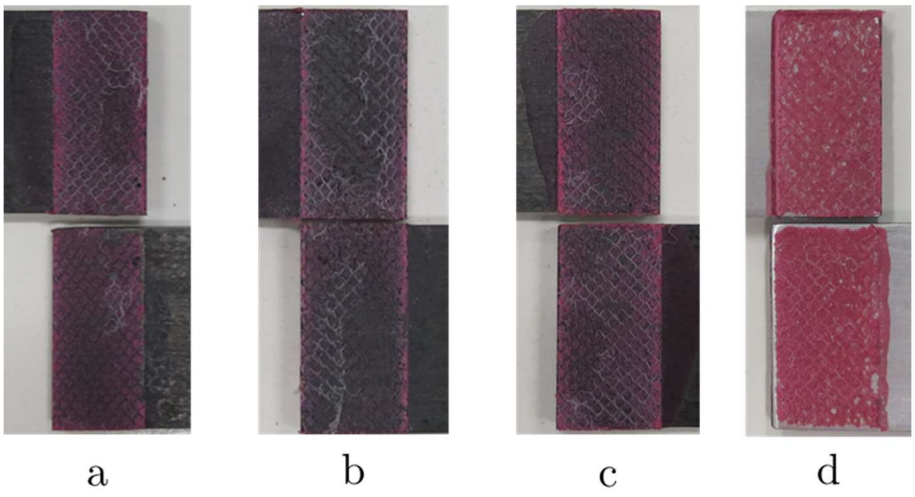

Figure 61 - Comparison of the failure surfaces for 12.5 mm overlap: (a) CFRP-only; (b) CFRP-Al-CFRP; (c) CFRP-Al-CFRP-Al-CFRP; (d) Al-CFRP-Al

For the 12.5 mm overlap, the difference in the experimental failure loads between the configurations are not representative, with the values of the different configurations falling within the standard deviation of the failure load of CFRP-only composite. The improvements in the failure load verified for the CFRP-Al-CFRP and the CFRP-Al-CFRP-Al-CFRP configurations were 3.51% and 3.75%, respectively. This was expected since the failure was cohesive in all specimens, so the joint strength would be more dependent on the adhesive rather than the adherends. The only exception is the configuration with aluminium on tops. Despite all the failures being cohesive, the failure load in this case is 12.93% lower than the reference joint. In this case the failure was mostly cohesive, but adhesive in small some areas. This may influence the failure load of the adhesive, and explain its decrease. Also, and although the manufacturing parameters were kept constant throughout the entire project, the thickness of the adherends might not be the same for every specimen. This influences not only the through-thickness properties of the adherends but also the final thickness of the adhesive during the manufacture of SLJ. Studies on the effect of adhesive thickness of epoxy structural adhesives in the joint strength concluded that the optimum strength is achieved for thicknesses between 0.1 and 0.5 mm [62]. If this thickness is not assured, the optimum joint strength may not be guaranteed.

4.3.2. SLJ's, 50 mm overlap

Following the same procedure, the failure loads, the joint strength and the type of failure for the 50 mm overlap are presented together in Table 11, with the failure surfaces for each configuration presented again in Figure 62.

Table 11 - Failure load and type of failure for the joints with a 50 mm overlap

Type	Average failure load [kN]	Joint strength [MPa]	Failure type
	37.66 ± 1.89	30.13 ± 1.51	Delamination
	39.75 ± 0.70	31.80 ± 0.56	Delamination
	40.39 ± 0.13	32.31 ± 0.10	Delamination
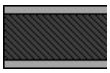	39.48 ± 0.31	31.58 ± 0.27	Cohesive + Adhesive

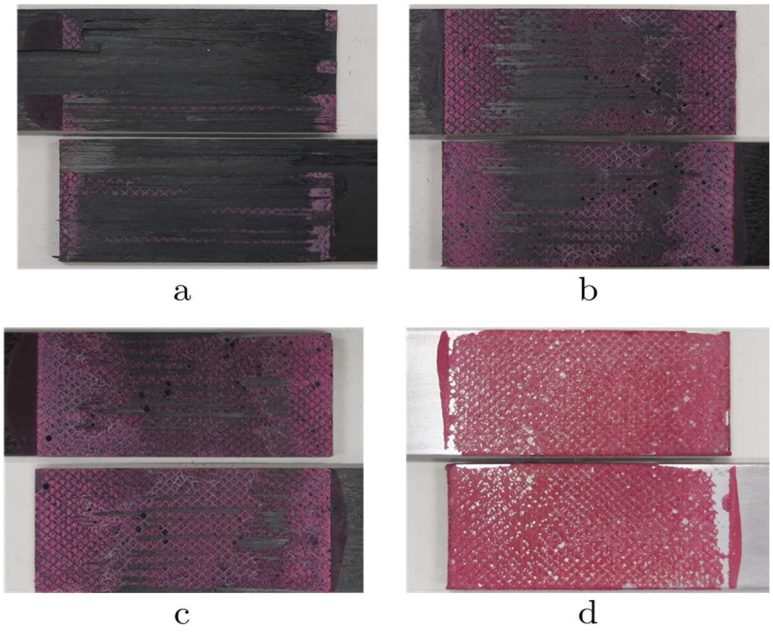

Figure 62 - Comparison of the failure surfaces for 50 mm overlap: (a) CFRP-only; (b) CFRP-Al-CFRP; (c) CFRP-Al-CFRP-Al-CFRP; (d) Al-CFRP-Al

For the 50 mm overlap, the reference joint suffered delamination, as it was discussed previously. With the configurations CFRP-Al-CFRP and CFRP-Al-CFRP-Al-CFRP, the failure mechanism was also delamination, but less severe when in comparison with the reference joint (see Figure 62). This suggests an increase in the peel strength of the adherends, since the peel stresses are the major cause for the occurrence of delamination [23]. Regarding joint strength, it was also verified an increase in the failure load, more significant than the increases for the 12.5 mm overlap; 5.55% for the CFRP-Al-CFRP lay-up and 7.25% for the CFRP-Al-CFRP-Al-CFRP. The increase in joint strength for the CFRP-Al-CFRP-Al-CFRP configuration was the most significant.

The failure mechanism was different for the Al-CFRP-Al configuration. The failure was cohesive in the adhesive, indicating a further improvement in the through-thickness properties relatively to the other configurations. The fact that the CFRP layer is located further away than the adhesive layer reduces the effect of the peel stresses at the edges of the overlap in the CFRP. Since the failure was cohesive, and despite the presence of an adhesive failure in some points, it was expected a more significant increase in the lap shear strength, correspondent to the shear strength value for the adhesive. However, this increase was not as expected, and was very similar to the ones from the other configurations (4.83%).

5. Numerical Analysis

Numerical analysis plays a major role in terms of mechanical project and testing. It is an easy way to simulate the mechanical behaviour of materials and components without the need of destructive tests, and also an outstanding tool when it comes to the preliminary steps of designing a structure, avoiding expensive prototypes that do not comply with the requirements. The major drawback of this techniques is the time it takes to obtain results, which is proportional to the discretization of the mesh; the more refined the mesh is, the longer it takes to obtain results, although they are more accurate.

5.1. Model description

Using Abaqus® 6.13 software, it was developed a 2D model to predict the failure loads and the failure type for each FML configuration. The adherends were modelled using a 4-node bilinear plane strain elements, CPE4R. The adhesive layer was modelled using 4-node two dimensional cohesive element, COH2D4.

Abaqus uses a triangular traction-separation law to simulate the damage in the adhesive (Figure 17), which has been explained in section 2.5.2. Despite the fact the adhesive in study is semi-ductile, this type of law is still adequate for this type of adhesive. Also, for implementing a trapezoidal separation law that could replicate better the ductile behaviour of the adhesive, sub-routines were required, which for the time of the project could not be developed in time.

In order to allow delamination of the CFRP, another cohesive zone was included in the model. This layer was 0.02 mm thick and was placed at 0.15 mm from the adhesive, which corresponds to the thickness of a pre-preg layer of CFRP (Figure 63). In the particular case of the Al-CFRP-Al configuration, it was placed at 0.15 mm from the aluminium part that was in contact with the adhesive.

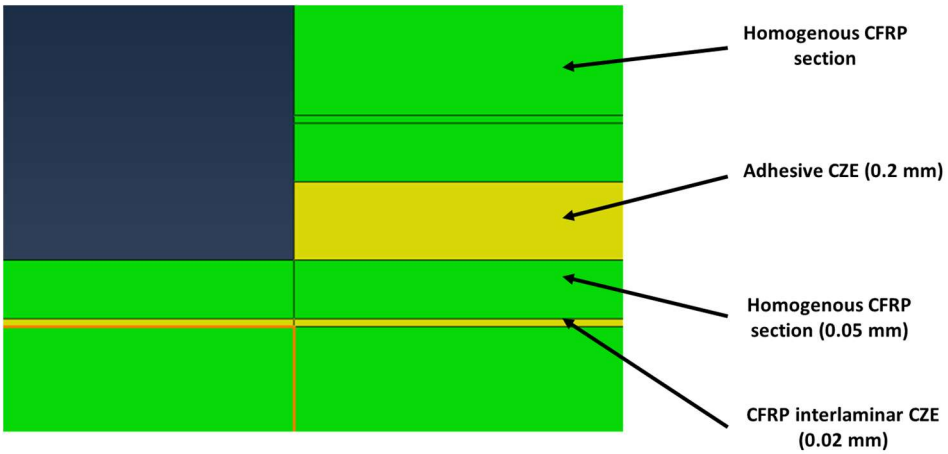

Figure 63 - Distribution of the CZE layers throughout the SLJ

The cohesive parameters to define the CFRP traction separation law for both mode I and II solicitations are presented in Table 12. The cohesive parameters for the adhesive were already shown in the chapter 4.

Table 12 - Cohesive parameters for CFRP interlaminar failure

	Mode I	**Mode II**
$\boldsymbol{\sigma_R}$ **[MPa]**	32	30
$\boldsymbol{G_c}$ **[N/mm]**	0.66	1.13

Regarding the boundary conditions of the model, a schematic representation is presented in Figure 64. At the right end of the joint was applied a constant displacement, while the left end was fixed in every direction. Also, for both edges the movement was limited in the vertical direction, representing the forces imposed by the clamps during the test.

Figure 64 - Schematic view of the boundary conditions imposed for the numerical model

The thermal residual stresses due to the difference in the thermal expansion coefficient between CFRP and aluminium are a major concern for this type of material [27]. For a more realistic model, an intermediate step before applying the displacement is created, with the cure temperature of the adhesive. In the following step room temperature is imposed. This difference in temperature will simulate the effect of the cure of the adhesive in the FML, and consider the thermal residual stresses existent in the adherends. The CTE for CFRP was considered 0 m/m K^{-1}.

5.2. Numerical results

The load displacement curves obtained from the FEA for both 12.5 and 50 mm are compared with experimental ones in Figure 65.

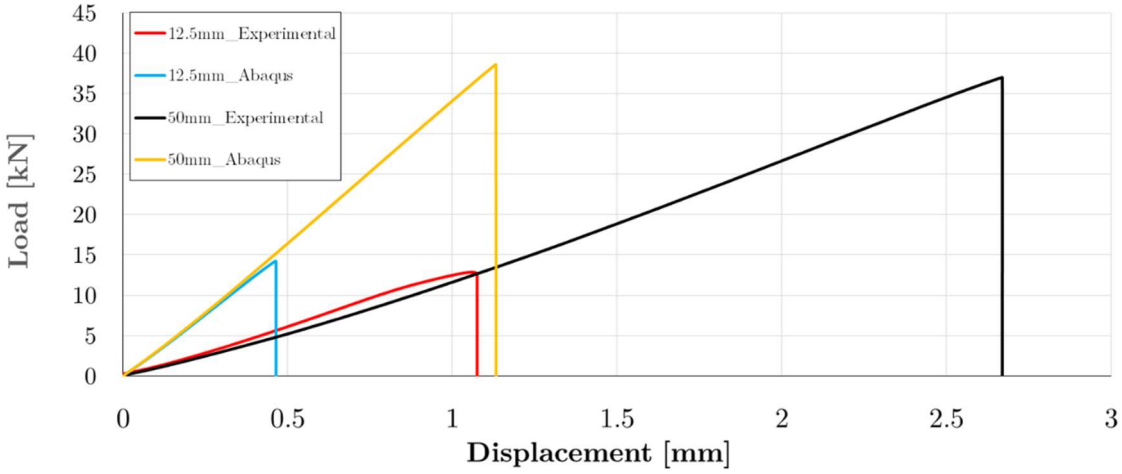

Figure 65 - Comparison between the experimental and the FEA load vs displacement curves for CFRP-only specimens

The failure load obtained in FEA was 14.53 kN for the 12.5 mm overlap and 38.57 kN for the 50 mm overlap, against 12.53 ± 0.40 kN and 37.66 ± 1.89 kN for the experimental results. Despite the fact that the predictions are slightly higher, the model can be considered accurate and is able to give a good prediction for the failure load.

The differences in the slope between the numerical model and the experimental results can be explained by the stiffness of the gripping system, since the displacement measured by the machine is affected by the stiffness of the tool steel setup used to fix the specimens.

In order to verify if the differences in the slope are only due to the stiffness of the gripping system, a steel specimen with the same thickness was tested. Then, to the displacement measured was removed the displacement from only the steel, calculated using Hooke's Law. The resultant displacement is then the contribution from the gripping system. If this displacement is subtracted to the total displacement, it is possible to obtain the load vs displacement curve from the specimen only. This correction is depicted in Figure 66, for the CFRP-only specimens. The same methodology can be applied for all the specimens.

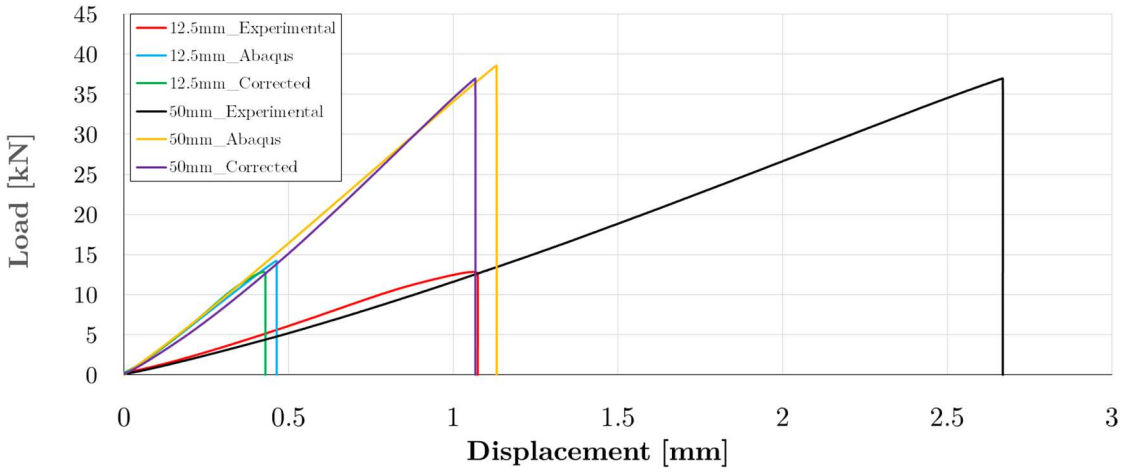

Figure 66 - Correction of the load vs displacement curves for CFRP-only specimens

Regarding the failure type, the damage distribution of the CZE in the moment of rupture indicates if the failure was cohesive in the adhesive or if there was delamination. The failure in the simulation occurs when the scalar stiffness degradation variable (SDEG) reaches 1. In Table 13 it is possible to compare the type of failure predicted by the FEA analysis and the failure surfaces for both overlaps.

Table 13 - Comparison between the failure types obtained by FEA and experimentally for the CFRP-only configuration

Overlap	FEA	Failure Surface	Failure
12.5 mm	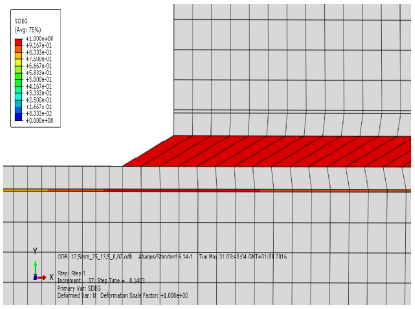	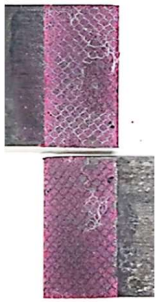	Cohesive
50 mm	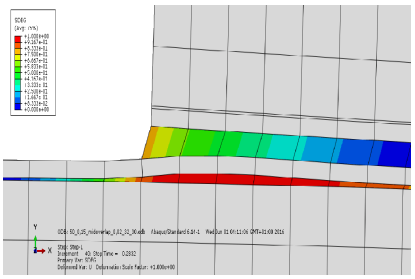	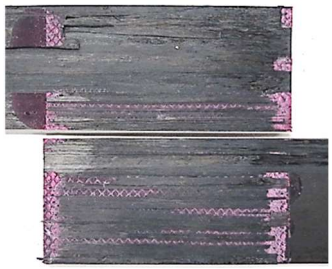	Delamination

In the numerical models, for the 12.5 mm overlap, the failure occurs first in the adhesive, with the CZE in the carbon fibre already damaged. For the 50 mm overlap, it is clear that the damage in the CZE of the carbon fibre reaches its peak first, while there is already some damage in the adhesive at the edges of the overlap. This results are coherent with the experimental data, where it was evident the delamination of the adherends, with the adhesive at this edges showing a slightly different colour than the rest of the bonded length, indicating some plastic deformation. This is explained by the stress concentration on the edges of the bonded area, where the peel stresses are maximum.

Now comparing the numerical results for the aluminium-carbon fibre configurations, both CFRP-Al-CFRP and CFRP-Al-CFRP-Al-CFRP configurations presented the same behaviour as the CFRP-only configuration. The failure was cohesive in the adhesive for the 12.5 mm overlap and delamination in the composite occurred for the 50 mm overlap. Regarding the Al-CFRP-Al configuration, in Table 14 are presented

the failure types predicted by the FEA and the fracture surface obtained experimentally for this lay-up.

Table 14 - Comparison between the failure types obtained by FEA and experimentally for the Al-CFRP-Al lay-up

Overlap	FEA	Failure Surface	Failure
12.5 mm	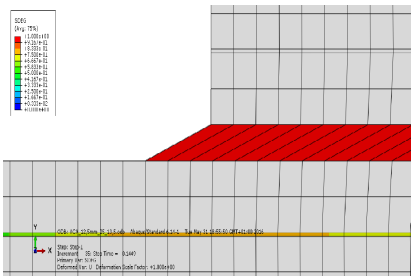		Cohesive
50 mm	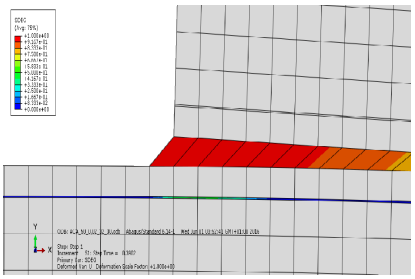	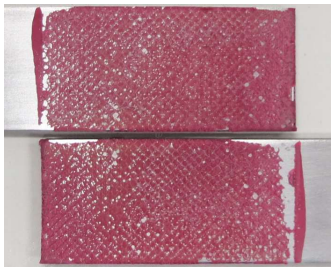	Cohesive

As obtained experimentally, the FEA analysis for the Al-CFRP-Al lay-up resulted in a cohesive failure for both overlaps. In both cases there is already some damage in the CFRP cohesive layer, but it is clear that the failure occurs in the adhesive. It is possible to conclude that all the models predicted correctly the failure mode for all the lay-up configurations and overlaps.

6. Discussion

In Figure 67 and Figure 68 a comparison is made between the experimental results and the FEA predictions for the failure load of the SLJ's.

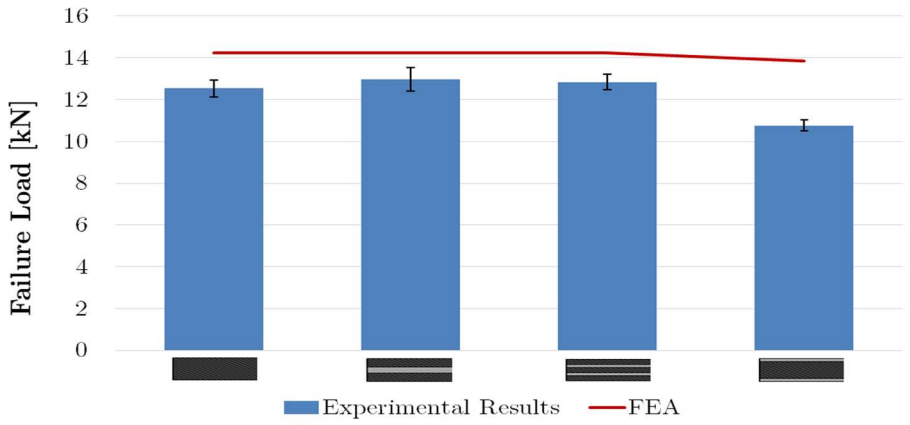

Figure 67 - Comparison between FEA predictions and experimental results for the failure load of specimens with a 12.5 mm overlap

For the 12.5 mm overlap, all the predictions were coherent with the experimental results, although with a higher failure load. The bigger decrease verified for Al-CFRP-Al in comparison with the other configurations was also verified using FEA, although in a smaller scale. Also, the fact that the failure in the adhesive for this lay-up was not completely cohesive (there was some small areas with an adhesive failure) may contribute to this difference.

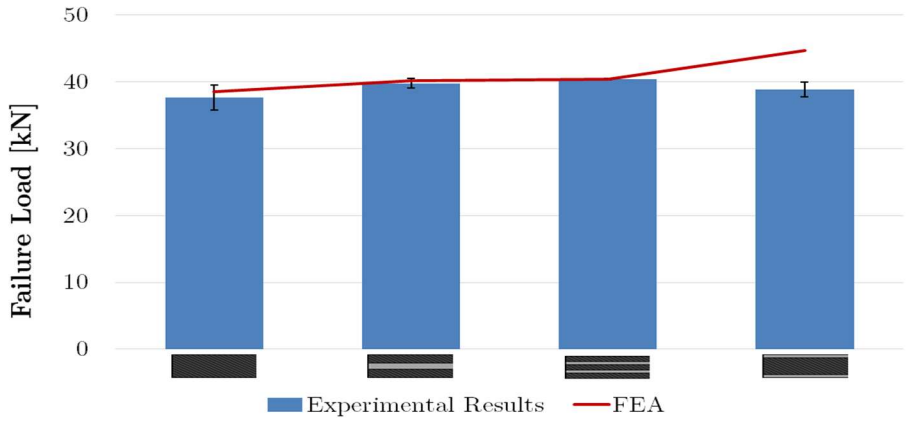

Figure 68 - Comparison between FEA predictions and experimental results for the failure load of specimens with a 50 mm overlap

For the 50 mm overlap, the trend of the predictions match quite accurately the experimental results obtained for first three lay-ups. Regarding the Al-CFRP-Al, in this case the predictions was significantly higher in comparison to the experimental results. This indicates that, even though the failure was cohesive, the adhesive is not working up to its full potential. As said previously, this configuration did not behaved as expected for both overlaps, having lower failure loads than the other configurations. Besides the eventual problem of the adhesive thickness, for this configuration it is the aluminium that bonds with the adhesive, whereas in the other lay-ups it is the carbon fibre that bonds with the adhesive. The aluminium surfaced that was bonded with the adhesive was not anodized (the aluminium sheets were anodized to produce the laminates, but after the cure of the laminate and the further abrasion and degreasing the anodized layer is eliminated), because it is not possible to anodize the aluminium already bonded with the carbon fibre. Following these results, the aluminium may require a superior surface treatment other than sand abrasion and degreasing prior to the bonding. Technologies such as sol-gel or more advanced treatments may improve the bonding between the adhesive and the aluminium and thus increase the joint strength for this configuration. Although most used for durability purposes, primers could also be a solution to eliminate the adhesive failure and further improve the bonding quality.

Another factor that influences all the joints was the way the cure was performed. Since this adhesive was specific designed for the aviation industry, it was formulated for a cure using an autoclave, a widespread method to cure components for this type of applications. A cure performed with an autoclave is more effective when in comparison with a hot plates press, since it avoids the presence of air bubbles and voids that can modify drastically the behaviour of the adhesive. Unfortunately during this project it was the only resource available to manufacture the SLJ's.

7. Conclusions and future works

7.1. Conclusions

The purpose of this project was to find the best lay-up configuration using hybrid aluminium-carbon fibre laminates that increased the peel strength of a CFRP joint. For achiving this goal, a complet characterization of an aeronautical adhesive was performed in order to accurately simulate the mechanical behaviour of SLJ with the different configurations. All the hybrid laminates were produced and the respective SLJ were tested to evaluet the joint strenght and the failure mode.

For all the 12.5 mm overlap SLJ the failure was cohesive in the adhesive, with no relevant improvements in the joint strength. Regarding the 50 mm overlap, there was clear delamination of the CFRP specimens with the adhesive studied. By adding one or two aluminium sheets to the CFRP composite, there was an evident decrease in the severity of the delamination. There was a small increase in the joint strength for the new configurations. Using the Al-CFRP-Al, for the 50 mm overlap there is no delamination and the failure mode is cohesive in the adhesive.

The numerical models correlated well with every configuration studied, for both overlaps, with a correct prediction of the failure modes and an accurate prediction of the failure loads. A bigger increase in the failure load using Al-CFRP-Al was determined, and this configuration was proven to be the best in terms of the severity of the delamination.

7.2. Future works

In order to continue the work developed in this thesis, some suggestions are proposed below with the purpose of better understanding the behaviour of FML and its properties:

-Try different surface treatments for aluminium with the purpose of improving the bond strength between this material and the adhesive.

-test different FML configurations using FEA to assess their effectiveness in terms of reducing the peel stresses, as well as other ratios between metal and CFRP.

-use a different metal to produce the FML. Because of its low weight and excellent mechanical properties, and as referred in this thesis, titanium is a natural candidate for this proposal.

-evaluate the bonding between the titanium and the CFRP and study surfaces treatments that might improve bond strength.

-study the durability of the bond between adhesive and FML and compare the effects of the different surfaces treatments.

-develop a trapezoidal law in order to better simulate the ductile behaviour of the adhesive.

References

[1] P. P. Camanho, A. Fink, A. Obst, and S. Pimenta, "Hybrid titanium–CFRP laminates for high-performance bolted joints," *Composites Part A: Applied Science and Manufacturing,* vol. 40, pp. 1826-1837, 12// 2009.

[2] A. P. Mouritz, "Review of z-pinned composite laminates," *Composites Part A: Applied Science and Manufacturing,* vol. 38, pp. 2383-2397, 12// 2007.

[3] L. F. M. da Silva and R. D. Adams, "Techniques to reduce the peel stresses in adhesive joints with composites," *International Journal of Adhesion and Adhesives,* vol. 27, pp. 227-235, 4// 2007.

[4] T. Sinmazçelik, E. Avcu, M. Ö. Bora, and O. Çoban, "A review: Fibre metal laminates, background, bonding types and applied test methods," *Materials & Design,* vol. 32, pp. 3671-3685, 8// 2011.

[5] S. Wu, *Polymer interface and adhesion*. New York: M. Dekker, 1982.

[6] A. J. Kinloch, *Adhesion and adhesives science and technology*. London: Chapman And Hall, 1987.

[7] W. Brockmann, P. L. Geiß, J. Klingen, and B. Schröder, *Adhesive Bonding: Materials, Applications and Technology*, 2009.

[8] R. D. Adams, *Adhesive bonding science, technology and applications*. Boca Raton: CRC, 2005.

[9] S. Ebnesajjad, *Handbook of Adhesives and Surface Preparation*, 2011.

[10] *Engineered materials handbook*. Metals Park, Ohio: ASM International, 1987.

[11] L. F. M. da Silva, A. Öchsner, and R. D. Adams, *Handbook of adhesion technology*. Heidelberg: Springer-Verlag, 2011.

[12] E. A. S. Marques, D. N. M. Magalhães, and L. F. M. da Silva, "Experimental study of silicone-epoxy dual adhesive joints for high temperature aerospace applications," *Materialwissenschaft und Werkstofftechnik,* vol. 42, pp. 471-477, 2011.

[13] A. Kaya, M. S. Tekelioğlu, and F. Findik, "Effects of various parameters on dynamic characteristics in adhesively bonded joints," *Materials Letters,* vol. 58, pp. 3451-3456, 11// 2004.

[14] M. T. Aronhime and J. K. Gillham, *Time-temperature-transformation (TTT) cure diagram of thermosetting polymeric systems*, 1986.

[15] R. J. C. Carbas, L. F. M. da Silva, E. A. S. Marques, and A. M. Lopes, "Effect of post-cure on the glass transition temperature and mechanical properties of epoxy adhesives," *Journal of Adhesion Science and Technology,* vol. 27, pp. 2542-2557, 2013.

[16] Y. Zhang, R. D. Adams, and L. F. M. da Silva, "A rapid method of measuring the glass transition temperature using a novel dynamic mechanical analysis method," *Journal of Adhesion,* vol. 89, pp. 785-806, 2013.

[17] S. H. Myhre, J. D. Labor, and S. C. Aker, "Moisture problems in advanced composite structural repair," *Composites,* vol. 13, pp. 289-297, 7// 1982.

[18] C. D. L. P. P. M. C. E. Environments, N. M. A. Board, D. E. P. Sciences, and N. R. Council, *Going to Extremes: Meeting the Emerging Demand for Durable Polymer Matrix Composites*: National Academies Press, 2005.

[19] A. Saleem, L. Frormann, and A. Iqbal, "High performance thermoplastic composites: Study on the mechanical, thermal, and electrical resistivity properties of carbon fiber-reinforced polyetheretherketone and polyethersulphone," *Polymer Composites,* vol. 28, pp. 785-796, 2007.

[20] D. Gay, S. V. Hoa, and S. W. Tsai, *Composite Materials: Design and Applications*: CRC Press, 2002.

[21] R. D. Adams, J. Comyn, and W. C. Wake, *Structural Adhesive Joints in Engineering*: Springer, 1997.

[22] M. D. Banea and L. F. M. da Silva, "Adhesively bonded joints in composite materials: An overview," *Proceedings of the Institution of Mechanical Engineers, Part L: Journal of Materials: Design and Applications,* vol. 223, pp. 1-18, 2009.

[23] L. J. Hart-Smith, "Adhesive-bonded single-lap joints," *NASA Langley contract report NASA CR-112236,* 1973.

[24] J. J. Homan, "Fatigue initiation in fibre metal laminates," *International Journal of Fatigue,* vol. 28, pp. 366-374, 4// 2006.

[25] S. E. Moussavi-Torshizi, S. Dariushi, M. Sadighi, and P. Safarpour, "A study on tensile properties of a novel fiber/metal laminates," *Materials Science and Engineering: A,* vol. 527, pp. 4920-4925, 7/15/ 2010.

[26] (2005) Creating a Titan. *Flight International*.

[27] J. Xue, W.-X. Wang, Y. Takao, and T. Matsubara, "Reduction of thermal residual stress in carbon fiber aluminum laminates using a thermal expansion clamp," *Composites Part A: Applied Science and Manufacturing,* vol. 42, pp. 986-992, 8// 2011.

[28] B. Kolesnikov, L. Herbeck, and A. Fink, "CFRP/titanium hybrid material for improving composite bolted joints," *Composite Structures,* vol. 83, pp. 368-380, 6// 2008.

[29] P. Cortés and W. J. Cantwell, "The prediction of tensile failure in titanium-based thermoplastic fibre–metal laminates," *Composites Science and Technology,* vol. 66, pp. 2306-2316, 10// 2006.

[30] J. J. Mazza, "Sol-gel technology for low-voc, nonchromated adhesive bonding applications," 2004.

[31] G. W. Critchlow and D. M. Brewis, "Review of surface pretreatments for aluminium alloys," *International Journal of Adhesion and Adhesives,* vol. 16, pp. 255-275, 1996/01/01 1996.

[32] A. Bjørgum, F. Lapique, J. Walmsley, and K. Redford, "Anodising as pre-treatment for structural bonding," *International Journal of Adhesion and Adhesives,* vol. 23, pp. 401-412, // 2003.

[33] W. Brockmann, O. D. Hennemann, H. Kollek, and C. Matz, "Adhesion in bonded aluminium joints for aircraft construction," *International Journal of Adhesion and Adhesives,* vol. 6, pp. 115-IN1, 7// 1986.

[34] A. Kurtovic, E. Brandl, T. Mertens, and H. J. Maier, "Laser induced surface nano-structuring of Ti–6Al–4V for adhesive bonding," *International Journal of Adhesion and Adhesives,* vol. 45, pp. 112-117, 9// 2013.

[35] O. Volkersen, "Die niektraftvertleiling in zugheanspruchten mit konstanten laschenquerschritten," *Luftfartfoeshing,* vol. 15, p. 41, 1938.

[36] L. F. M. da Silva, *Modeling of Adhesively Bonded Joints*: Springer Berlin Heidelberg, 2008.

[37] M. Goland and E. Reissner, "The stresses in cemented joints," *J. Appl. Mech,* vol. 11, pp. 11-27, 1944.

[38] V. Mallick, *Stress Analysis of Metal/CFRP Adhesive Joints Subjected to the Effects of Thermal Stress*: University of Bristol, 1989.

[39] L. F. M. da Silva, P. J. C. das Neves, R. D. Adams, and J. K. Spelt, "Analytical models of adhesively bonded joints—Part I: Literature survey," *International Journal of Adhesion and Adhesives,* vol. 29, pp. 319-330, 4// 2009.

[40] M. Scotch-Weld, "AF 163-2 Structural Adhesive Film, Technical Datasheet " 2009.

[41] L. F. M. da Silva and R. D. S. G. Campilho, *Advances in Numerical Modeling of Adhesive Joints*: Springer Berlin Heidelberg, 2011.

[42] R. D. Adams and J. A. Harris, "The influence of local geometry on the strength of adhesive joints," *International Journal of Adhesion and Adhesives,* vol. 7, pp. 69-80, 1987/04/01 1987.

[43] F. J. P. Chaves, L. F. M. da Silva, M. F. S. F. de Moura, D. A. Dillard, and V. H. C. Esteves, "Fracture Mechanics Tests in Adhesively Bonded Joints: A Literature Review," *The Journal of Adhesion,* vol. 90, pp. 955-992, 2014/11/02 2014.

[44] M. Ortiz and A. Pandolfi, "Finite-deformation irreversible cohesive elements for three-dimensional crack-propagation analysis," *International Journal for Numerical Methods in Engineering,* vol. 44, pp. 1267-1282, 1999.

[45] C. D. M. Liljedahl, A. D. Crocombe, M. A. Wahab, and I. A. Ashcroft, "Damage modelling of adhesively bonded joints," *International Journal of Fracture,* vol. 141, pp. 147-161, 2006.

[46] J. P. M. Gonçalves, M. F. S. F. d. Moura, P. M. S. T. d. Castro, and A. T. Marques, "Interface element including point-to-surface constraints for three-dimensional problems with damage propagation," *Engineering Computations,* vol. 17, pp. 28-47, 2000.

[47] M. F. S. F. de Moura, R. D. S. G. Campilho, and J. P. M. Gonçalves, "Crack equivalent concept applied to the fracture characterization of bonded joints under pure mode I loading," *Composites Science and Technology,* vol. 68, pp. 2224-2230, 8// 2008.

[48] L. F. M. da Silva, D. A. Dillard, B. Blackman, and R. D. Adams, *Testing adhesive joints best practices*. Weinheim: Wiley-VCH Verlag GmbH & Co. KGaA, 2012.

[49] M. F. S. F. de Moura and A. B. de Morais, "Equivalent crack based analyses of ENF and ELS tests," *Engineering Fracture Mechanics,* vol. 75, pp. 2584-2596, 6// 2008.

[50] M. F. S. F. de Moura, R. D. S. G. Campilho, and J. P. M. Gonçalves, "Pure mode II fracture characterization of composite bonded joints," *International Journal of Solids and Structures,* vol. 46, pp. 1589-1595, 3/15/ 2009.

[51] J. P. Sargent, "Durability studies for aerospace applications using peel and wedge tests," *International Journal of Adhesion and Adhesives,* vol. 25, pp. 247-256, 6// 2005.

[52] R. D. S. G. Campilho, *Repair of composite and wood structures*. Porto: [s. n.], 2009.

[53] C. Matz, "Optimization of the durability of structural titanium adhesive joints," *International Journal of Adhesion and Adhesives,* vol. 8, pp. 17-24, 1988/01/01 1988.

[54] R. O. Ritchie, W. Yu, and R. J. Bucci, "Fatigue crack propagation in ARALL® LAMINATES: Measurement of the effect of crack-tip shielding from crack bridging," *Engineering Fracture Mechanics,* vol. 32, pp. 361-377, 1989/01/01 1989.

[55] T. J. d. Vries and C. A. J. R. Vermeeren, *R-curve testdata: 2024-T3, 7075-T6, GLARE 2 and GLARE 3*. Delft: Delft University of Technology, 1995.

[56] "NF T 76-142 Standard," in *Méthode de préparation de plaques d'adhésifs structuraux pour la réalisation d'éprouvettes d'éssai de caractérisation*, ed. France, 1988.

[57] "ISO 11003-2 Standard," in *Adhesives - determination of shear behaviour of strucutral bonds - part 2: thick-adherend tensile-test method*, ed. Switzerland, 1993.

[58] "ASTM 3433-99," in *Standard Test Method for Fracture Strength in Cleavage of Adhesives in Bonded Metal Joints*, ed. USA, 2012.

[59] "ASTM 3933-98," in *Standard Guide for Preparation of Aluminum Surfaces for Structural Adhesives Bonding (Phosphoric Acid Anodizing)*, ed. USA, 2010.

[60] D. O. Adams and D. F. Adams, "Tabbing guide for composite test specimens," U.S. Department of Transportation, Federal Aviation Admininstration2002.

[61] A. A. Zadpoor, J. Sinke, and R. Benedictus, "Elastoplastic deformation of dissimilar-alloy adhesively-bonded tailor-made blanks," *Materials & Design,* vol. 31, pp. 4611-4620, 12// 2010.

[62] D. M. Gleich, M. J. L. Van Tooren, and A. Beukers, "Analysis and evaluation of bondline thickness effects on failure load in adhesively bonded structures," *Journal of Adhesion Science and Technology,* vol. 15, pp. 1091-1101, 2001.